A sodium channel gating model based on single channel, macroscopic ionic, and gating currents in the squid giant axon

C. A. Vandenberg* and F. Bezanilla‡

*Department of Biological Sciences and Neurosciences Research Institute, University of California, Santa Barbara, California 93106; and ‡Department of Physiology, Ahmanson Laboratory of Neurobiology and Jerry Lewis Neuromuscular Research Center, University of California, Los Angeles, California 90024

ABSTRACT Sodium channel gating behavior was modeled with Markovian models fitted to currents from the cut-open squid giant axon in the absence of divalent cations. Optimum models were selected with maximum likelihood criteria using single-channel data, then models were refined and extended by simultaneous fitting of macroscopic ionic currents, ON and OFF gating currents, and single-channel first latency densities over a wide voltage range. Best models have five closed states before channel opening, with inactivation from at least one closed state as well as the open state. Forward activation rate constants increase with depolarization, and deactivation rate constants increase with hyperpolarization. Rates of inactivation from the open or closed states are generally slower than activation or deactivation rates and show little or no voltage dependence. Channels tend to reopen several times before inactivating. Macroscopic rates of activation and inactivation result from a combination of closed, open and inactivated state transitions. At negative potentials the time to first opening dominates the macroscopic current due to slow activation rates compared with deactivation rates: channels tend to reopen rarely, and often inactivate from closed states before they reopen. At more positive potentials, the time to first opening and burst duration together produce the macroscopic current.

INTRODUCTION

The complex kinetic structure of the voltage-dependent sodium channel has been studied in detail, leading to a variety of mechanisms to explain the transient voltage-dependent activation of the sodium conductance that is followed more slowly by inactivation. Analysis of macroscopic ionic currents, gating currents, and single-channel currents each have revealed different aspects of the gating process. Our approach was to combine measurement of all three expressions of channel function to develop a model of channel gating.

Based on observations of macroscopic ionic currents, a number of models have been advanced to explain the relationship between channel activation and inactivation. Hodgkin and Huxley (1952) proposed independent mechanisms for activation and inactivation. Later, several authors proposed that inactivation may be coupled to activation (Goldman and Schauf, 1972; Bezanilla and Armstrong, 1977; Armstrong and Gilly, 1979; Bean, 1981; Oxford, 1981; Goldman and Kenyon, 1982; see, however, Gillespie and Meves, 1980), and showed a lag in the development of inactivation consistent with this hypothesis.

Gating currents studies provided evidence for interactions between the activation and inactivation processes by demonstrating that the charge movement responsible for activation was immobilized by the inactivation process (Armstrong and Bezanilla, 1977; Nonner, 1980). Gating currents gave other important information on the number of transitions between closed states leading to the open state, on the charge movement during channel gating, and on the relative rates of gating charge movement and ionic current (see Armstrong, 1981; Bezanilla, 1985).

Single-channel recordings have been useful in defining the relationship between the open state(s) and the closed states near the conducting state. Single-channel studies from mammalian sodium channel have shown that channels may inactivate from open as well as closed states (Aldrich et al., 1983; Horn and Vandenberg, 1984; Kunze et al., 1985; Scanley et al., 1990) and have provided insight into processes underlying the macroscopic ionic currents (e.g., Patlak and Ortiz, 1986; Patlak et al. 1986). However, significant differences exist between studies and between preparations (see Horn and Vandenberg, 1986; Aldrich and Stevens, 1987; Gonoi and Hille, 1987; Kirsch and Brown, 1989), leading to apparent controversy in estimates of the contributions of activation and inactivation to the macroscopic ionic current, in the magnitudes and voltage dependences of their rates, and in the question of whether the inactivation rates are inherently voltage dependent or derive their voltage dependence from the activation process. In addition, analyses based on sodium single-channel data alone are relatively insensitive to transitions occurring far from the open state, limiting their ability to define a model of gating that includes the early voltage-dependent transitions between closed states.

Address correspondence to Dr. Vandenberg.

Until recently, it had not been possible to record single-channel currents from the squid giant axon, the preparation in which gating current has been most extensively studied, because the external membrane surface is surrounded by a Schwann cell layer. With the development of techniques to record single sodium channels from the internal face of the cut-open squid giant axon (Bezanilla, 1987), as well as gating currents and macroscopic ionic currents (Vandenberg and Bezanilla, 1991) it became possible to describe sodium channel gating kinetics using all three types of measurements on the same preparation.

Our approach was to use single-channel data with maximum likelihood analysis for comparison of models and for estimating rate constants (Horn and Lange, 1983; Horn and Vandenberg, 1984). This provided a method for statistically selecting a model that was compatible with single-channel data. The preferred single-channel model then was extended to incorporate macroscopic ionic and gating current data by simultaneously fitting currents over a wide voltage range.

This represents a first attempt to derive such a comprehensive model of sodium channel gating. To limit the scope of this endeavor, we have confined our study to rapid processes that can be measured in current records of <20-ms duration. This includes the majority of the activation, deactivation, and inactivation processes, but does not encompass slow inactivation kinetics. Similarly, we have confined our study to a 100-mV voltage range between -98 and $+2$ mV. At more positive potentials the squid sodium current shows evidence of substantial steady-state current, and the presence of more than one open state (Chandler and Meves, 1970; Oxford and Yeh, 1985; Bezanilla and Armstrong, 1977; Correa and Bezanilla, 1990; Bezanilla and Correa, 1991).

Preliminary accounts of this work have been published in abstract form (Vandenberg and Bezanilla, 1988, 1990).

METHODS

Sodium single channel, macroscopic ionic, and gating current were recorded with patch techniques from the cut-open squid giant axon as described in the accompanying paper (Vandenberg and Bezanilla, 1991). Recordings were made at 5°C in the absence of divalent cations using 546 Na ASW (external)//Patch ionic (internal) solution for ionic currents and patch gating external//patch gating internal solution for gating currents (Vandenberg and Bezanilla, 1991). All data have been corrected for linear leak and capacitative currents either by a P/-4 procedure (for macroscopic currents), or by subtracting average records in which no openings occurred (for single-channel currents). Single-channel records were filtered at 3.1 KHz through an 8-pole Bessel filter, and digitized at 20 μs sample intervals; macroscopic ionic data were filtered at 7 KHz and sampled at 8–20 μs intervals; and gating current data were filtered at 7 KHz and sampled at 6-μs intervals.

Single-channel data analysis

Single-channel current records were analyzed for transitions between closed and open states by setting a threshold halfway between the closed and open current amplitudes (Colquhoun and Sigworth, 1983). The time at which the current crossed threshold was estimated using linear interpolation between digitized current values. The sequence of openings and closings and the dwell time before each transition were determined for each record using a computer algorithm and confirmed by visual inspection. 474 current records were analyzed for voltage jumps to each test potential. Single-channel analysis was performed with data from a patch that contained one channel, as estimated by the absence of overlapping events in more than 3,000 records, as predicted from the binomial distribution (Colquhoun and Hawkes, 1983).

Maximum likelihood analysis

Single-channel data were analyzed with maximum likelihood estimation of rate constants (Horn and Lange, 1983; Horn and Vandenberg, 1984) using a computer program kindly provided to us by Dr. Richard Horn (Roche Institute, Nutley, NJ). Correction for missed transitions (Roux and Sauve, 1985) had been incorporated into the likelihood program, and was employed in some analyses as indicated in the Results. Parameters were estimated and the likelihood surface searched to obtain the maximum log(likelihood) using a variable metric method algorithm kindly provided by Dr. Kenneth Lange (University of California, Los Angeles). Standard errors of the rate constants were estimated from the covariance matrix obtained during the estimation of rate constants. Likelihood calculations and estimation of rate constants were made using 20–33 MHz 386-based microcomputers with math coprocessors, and typically required 4–18 h for each set of data at one voltage when missed events correction was not used. Five sets of single-channel data (474 records each) were analyzed for each model, for voltages of -58, -48, and -38 (two data sets), and -28 mV.

Models that were examined were branched and cyclic Markovian kinetic models (Korn and Horn, 1988; McManus et al., 1988). For cyclic models, nonindependent rate constants were determined by microscopic reversibility using estimated rate constants, such that the product of the rate constants around a cycle in the clockwise direction were equal to the product of the rate constants in the counterclockwise direction. Models with up to six states, and 12 independent rate constants were used in model testing. The models had one open state, because the open time was well described by a single exponential, and up to five closed and inactivated states arranged in a variety of ways.

Models were compared using likelihood ratios tests for nested models, that is, those models that were subhypothesis of a larger model (Horn and Lange, 1983; Horn and Vandenberg, 1984). For a pair of nested models, twice the difference between the maximum log(likelihood)s is distributed as chi squared. The number of degrees of freedom is equal to the difference between the number of free parameters in each model times the number of data sets tested (Horn and Lange, 1983). The P value, obtained from standard tables of chi squared upper-tail probabilities, indicates the probability that the two models are statistically distinguishable. A low value (e.g., $P < .05$) shows that the general model is statistically superior to the subhypothesis.

For nonnested models, Akaike's asymptotic information criterion (AIC) was used to rank models (Akaike, 1974; Horn and Vandenberg,

1984):

$$\text{AIC} = 2[(\text{number of free parameters per model}) \times (\text{number of data sets}) - \log(\text{maximum likelihood})].$$

The model with a lower AIC is considered better. This ranking provided a method to compare models that could not be evaluated with likelihood ratios.

Predicting single-channel properties from estimated rates

Single channel probability densities for channel open time, closed time, and time to first opening were calculated numerically using the rate constants estimated from maximum likelihood analysis (Horn and Lange, 1983; Colquhoun and Hawkes, 1983; Horn and Vandenberg, 1984). The initial probability distribution between states was first set appropriately for each theoretical density at a given holding potential. At 20-μs intervals thereafter, the probability was calculated that the channel would be found in each state, based on its probability distribution in the preceding interval and the rate constants for transitions between states. For each theoretical density, the appropriate transition rates were set equal to zero. For example, in calculating the closed time density for model 3 (below), at time zero the channel could be found in either of the closed states immediately adjacent to the open state (i.e., C_3 and I) with probabilities proportional to the rates of leaving the open state (i.e., probability of being in $C_3 = d/[d+f]$; probability of being in $I = f/[d+f]$). The transition rates leaving the open state (d and f) were then set equal to zero to calculate the closed-time density, so that only transitions among closed states contributed to the theoretical density. Predicted open and closed time densities were scaled to histograms of single-channel data according to their areas (Colquhoun and Sigworth, 1983), and the first 50 μs were not included to minimize errors due to missed brief transitions. The time to first opening density did not require scaling.

Numerical simulations were used for comparison of the predicted and measured number of openings per record. Several hundred thousand single-channel records of the same duration as the test pulse were simulated, using the estimated rate constants, and the numbers of predicted openings were tabulated. Single-channel simulations were performed using a program provided by Dr. R. Horn (Roche Institute, Nutley, NJ). This method was used because theoretical predictions of the number of openings per burst did not account for the finite length of the pulse and the possibility of channel reopening from the inactivated state.

Predicting macroscopic gating current from single-channel model

To extend the predicted rates derived from single-channel analysis over a wide voltage range, estimated rate constants were assumed to be a simple exponential function of voltage (Stevens, 1978), and were fitted by weighted least squares, with the weighting factor equal to the inverse of the estimated variances. The voltage dependence of the rates gave the effective valence, $q_{i,j}$, of the transition rate, $\lambda_{i,j}$, from state i to j:

$$\lambda_{i,j} = A_{i,j} \exp(q_{i,j}FV/RT),$$

where V is the applied voltage, $A_{i,j}$ is the zero-voltage value of the rate constant from states i to j, $q_{i,j}$ is the effective valence of the i to j transition rate, F is the Faraday constant, R is the gas constant, and T is the absolute temperature. For the purposes of gating currents, the total charge movement between each pair of states, i and j, is the sum of the effective valences for the voltage dependent forward and reverse rate constants ($q_{i,j} + q_{j,i}$). In accordance with Eyring rate theory (Woodbury, 1971), the location of the peak of the energy barrier between stable energy wells i and j is given by the relative magnitude of the effective valence for the forward and reverse rates, while the height of the energy barrier as seen from well i or j at zero voltage is related to the value $A_{i,j}$ or $A_{j,i}$, respectively.

Macroscopic gating currents were simulated using the numerical methods outlined for single-channel probability densities. Gating currents were calculated as the rate of charge movement during the voltage pulse, which was equal to the sum over all pairs of states of the charge movement between states times the probability of being in each state times the transition rate between the states;

$$\text{Gating} = \sum_{\text{all } i,j} (q_{i,j} + q_{j,i})[(S_i)(\lambda_{i,j}) - (S_j)(\lambda_{j,i})].$$

Fitting macroscopic ionic and gating currents

Macroscopic ionic activation and tail currents, ON and OFF gating currents, and single-channel first latency densities were fitted simultaneously over a wide voltage range using the parameter optimization program SCoPfit generously provided by us by Dr. Mailen Kootsey (Duke University Medical Center, Durham, NC). The program was modified to allow fitting of 30 data records with up to 20 adjustable parameters. Models were expressed as a series of equations for the time derivatives of the probability of being in each state. The state equations were numerically integrated by the Euler method, and the predicted gating currents, ionic currents, and first latency densities were calculated and compared to the measured currents.

The models were expressed as a series of differential equations equating the change in probability of being in each state with time to the probability of entering that state from all other states and of leaving that state to any other state.

$$d(S_i)/dt = [(S_1(\lambda_{1,i}) + \cdots + (S_k)(\lambda_{k,i})] - (S_i)[(\lambda_{i,1}) + \cdots + (\lambda_{i,k})],$$

for all i, where S_i is the probability of being in state i, k is the total number of states, and $\lambda_{i,k}$ is the rate for going from state i to state k. For state transitions that were not allowed by the model, the corresponding rate was set to zero. All rates were assumed to be exponential functions of voltage. For example, a summary of the state equations describing the expanded model (Fig. 10) is shown in Table 3.

Each current record was described by its appropriate probability and the parameters optimized during fitting were the zero-voltage rate $A_{i,j}$ and effective valence of each rate constant $q_{i,j}$. Additional free parameters were arbitrary scaling factors to account for differences in total number of channels between ionic and gating currents experiments performed on different patches. The total number of free parameters estimated were 21 (nine zero-voltage rates, nine voltage dependences and three scaling factors). The program adjusted the rate constants while it minimized the difference between the experimental points and the predicted current using a chi squared error function. To provide approximately equal weight to various data types ~100 data points were sampled from each record of ionic activation currents (five records), ionic tail currents (five records), ON gating currents (three records), OFF gating currents (five records), and single channel first latency densities (three records). Currents during the first 100 μs from all records were not included to eliminate rounding artifacts due to filtering of the data.

For ionic current data, the records were fitted to the probability of being in the open state, which was scaled by the instantaneous current voltage relationship (Fig. 3 of Vandenberg and Bezanilla, 1991)

multiplied by the number of channels in the patch, as estimated by the fitting. The function used to fit the first latency density was identical to the probability of being open except that the open state was made absorbing (i.e., the rates for transitions leaving the open state were made equal to zero). Gating currents were calculated as described above.

At the start of a voltage pulse, the initial probability distribution of channels between states was calculated based on the equilibrium value for the distribution at the holding potential. For tail currents and OFF gating currents, the probability distribution at the beginning of the tail was calculated from the distribution at the end of the activating pulse.

Because it was difficult to find a set of rate constants that could simultaneously fit all the data, the fitting procedure was done first in parts to provide good initial estimates of the parameters. The actual fitting procedure was done by allowing the algorithm to fit one third to one half of the parameters to a subset of the total data set, while holding the other parameters fixed, with the intention of obtaining initial estimates of the parameters that were most sensitive to that particular subset of data. The procedure was repeated with several overlapping subsets of parameters and data sets, and finally all the parameters were set free to adjust the fit of the entire data set. Repeated fits using different initial guesses for parameters and different initial subsets of data, converged on the same final set of rate constants.

RESULTS

Single-channel currents

Single channel currents recorded from the cut-open axon are shown in Fig. 1 for voltage pulses to −48 mV (*left panel*) or −28 mV (*right panel*). This patch contained only one active sodium channel, because in recordings from >3,000 depolarizing voltage pulses, simultaneous openings of more than one channel was not observed. From current records such as these, we see that the channel opened rapidly after the start of the voltage pulse (*arrows*), and the latency to first opening was shorter for the more depolarized test potential of −28 mV than for −48 mV. After the channel opened, it usually closed and reopened several times during the 22-ms voltage pulse. The channel openings tended to cluster early in the record, but there were occasional late reopenings occurring near the end of the record.

Data from this single-channel patch were used in the comparison of models with maximum likelihood analysis. Because this patch was stable for several hours, nearly 500 single-channel records at each potential were collected for voltage pulses to potentials from −58 mV to −8 mV in 10 mV increments. The average currents showed good agreement with macroscopic currents recorded at the same voltage, and the channel kinetics were stationary throughout the recording period, as measured by similarity in the single-channel properties for two sets of data at −38 mV recorded at the beginning and the end of the experiment.

Single-channel model comparison

To describe the gating behavior of the sodium channel, we used data from this single-channel patch to make quantitative comparisons of various models. The kinetic models used were all Markovian (Korn and Horn, 1988; McManus et al., 1988), and were restricted to have at most six states and 12 parameters. The constraints on

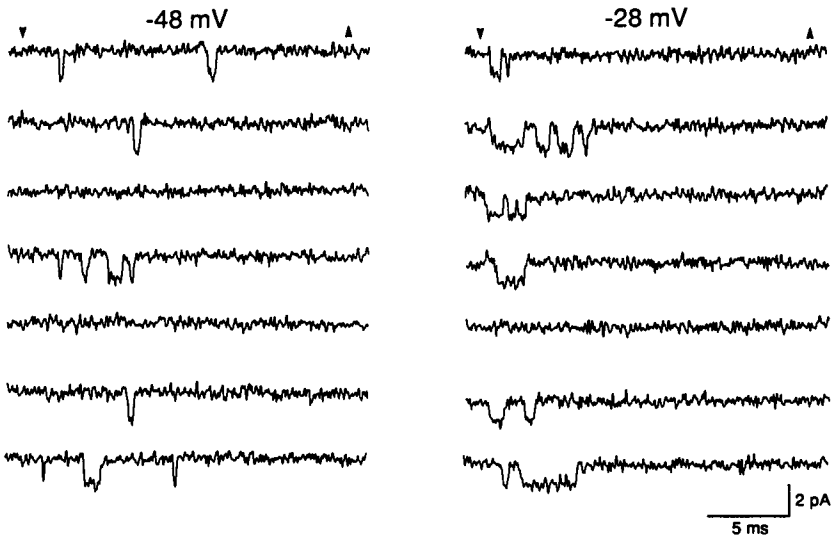

FIGURE 1 Single-channel currents used in modeling. Examples of single-channel current recordings are shown for voltage pulses to either −48 mV or −28 mV (beginning and end of pulse indicated by *arrowheads*) from a holding potential of −108 mV. The patch contained only one channel. Data were filtered at 3.1 KHz.

the number of states were necessary to obtain convergence on a unique solution during the maximum likelihood estimation.

A variety of models were compared, differing primarily in their arrangement of closed and inactivated states near the open state. The channels were assigned an initial location in C_1, the closed state farthest from the open state, because the membrane was held at a very negative potential, causing this closed states to be most populated. Calculation of the initial probability distribution based on the estimated rate constants indicated that this assumption was justified. To reduce the number of free parameters, the forward rate constants between the first two closed states were assigned to be equal, as were the reverse rates. When these rates were allowed to be independent, the minimization routine was unable to converge on a solution and parameters could not be estimated.

The models that were examined with the single-channel data are shown in Table 1, listed in order of their relative Log(likelihood). Comparisons of general models and their subhypotheses are shown in Table 2. Arrows between states indicate allowed transitions. Surprisingly, with a variety of pathways to choose from, many models had rates along one or more of the transition paths that were estimated to be essentially zero. Dotted lines between states indicate that the transition was allowed by the model, but for all voltages the rate was estimated as 10^{-5} s^{-1}, the lower bound used as the parameter constraint. This simplified model comparison, as these models had identical likelihoods to the corresponding models without the transition indicated by the dotted lines, and were therefore indistinguishable statistically by likelihood ratios. We examined the possibility that the absent transitions between states might be caused by an undetected slow-inactivated state. For example, in model 5 the C_2 to I transition rate might have been overestimated to account for blank records due to slow inactivation, causing an underestimation in the C_3 to I transition rate. This possibility was tested using the reversible model 3 by including a slow-inactivated state C_0 that did not communicate with the other states, but reduced the fraction of time the channel could be found in C_1 at the start of the pulse. This model did not represent a statistical improvement by likelihood ratios test ($P = 0.06, X^2 = 10.5$, degrees of freedom = 5), and the estimated probability of finding the channel in C_0 was not constant for identical starting conditions. This suggested that the channel was not slow inactivated, and the absence of some of the transition pathways represented a real phenomenon.

Examination of the data and comparison of the AIC ranking (Table 1) and likelihood ratios comparisons (Table 2) indicates general features that make some models preferable to other models:

(*a*) Inactivation occurs from closed states. Strictly coupled models in which channels must open before they inactivate from the closed states (models 8 and 9) are not acceptable. Inactivation from closed states is required, for example, to account for the records in which no channel opening occurs. The proportion of blank records is greater than would be expected by occasional long times to first opening, so some closed channels must inactivate before opening.

(*b*) Inactivation may occur from the open state. Models allowing inactivation from only the closed state C_3 (models 2 and 6) were nearly equivalent to models with inactivation from closed as well as open states (models 3 and 5). Among models without return from inactivation (models 5 and 6) the better model (model 5) allowed inactivation from the open state as well as the closed state C_2. However, when inactivation was allowed to be reversible, inactivation from closed state C_3 was sufficient to account for the single-channel data (model 2), and inactivation from the open state was not required (model 3).

(*c*) The best models allow inactivation to be reversible. Thus the superior models (models 1–4) permit return from the inactivated state to open and/or closed states. This return from inactivation permits recovery from inactivation upon return to negative holding potentials. It also allows for late reopenings during a depolarizing pulse after the peak sodium current has declined, and contributes to the steady-state sodium current. Because these data were derived from a patch with only one channel, it is apparent that at least some of the late reopenings are due to an inherent property of the channel and not due to a population of channels that have lost the ability to inactivate.

Slow return from an inactivated state is preferably to a fast-flickery closed state connected to the open state. Interestingly, for model 4, return from the closed state I_2 to the open state was slow, with return rates of 18–26 s^{-1}. Models were able to account for fast channel reopenings by utilizing the channel activation/deactivation pathway (C_1, C_2, and C_3) without the need for additional fast closings from the open state.

(*d*) More closed states produce better models. Additional closed states contribute to the lag in the time to first opening, and to the sigmoid rise in the probability of being open. The addition of another closed state to the left of C_1 (not shown) increased the log(likelihood) by ~5. However, for single-channel data there was too much uncertainty in estimating rate constants to use these larger models. Extra closed states also were required by the gating currents, and they were incorporated into the extended model (see below).

TABLE 1 Kinetic models

Model number	Model	Relative log(likelihood)	AIC rank	Numbers of parameters
1	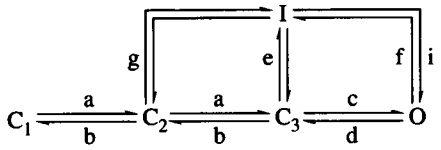	0	3	8
2	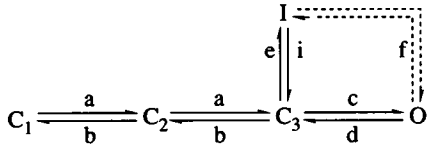	−4.0	1	7, (6)
3	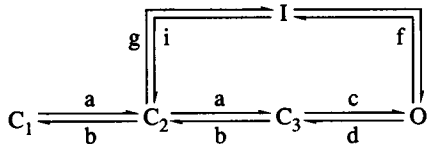	−4.1	2	7
4	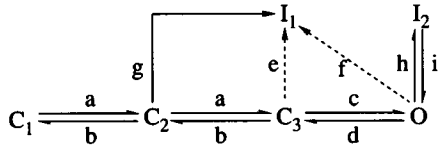	−219.8	4	9, (7)
5	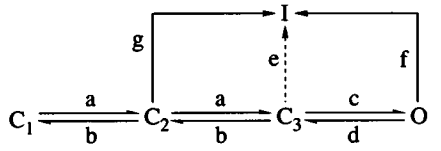	−354.6	5	7, (6)
6	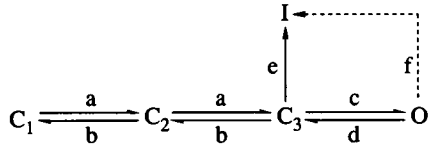	−363.7	6	6, (5)
7	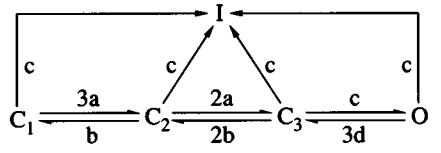	−844.1	7	3
8	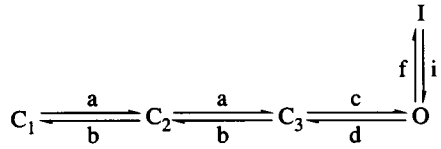	−1320.0	8	6
9	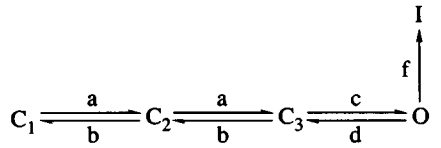	−1325.4	9	5

TABLE 2 **Comparison of nested models by likelihood ratios**

Subhypothesis model number*	X^2	Degrees of freedom	P value
	General model 1		
2	7.9	5	0.16
3	8.1	5	0.15
5	709.1	5	$<10^{-4}$
6	727.5	5	$<10^{-4}$
8	2640.0	10	$<10^{-4}$
9	2650.8	15	$<10^{-4}$
	General model 4		
5	269.6	10	$<10^{-4}$
6	288.0	15	$<10^{-4}$
	General model 5		
6	18.4	5	0.002

*Model number from Table 1 indicates full models including transitions marked with dashes.

(*e*) The Hodgkin and Huxley (1952) model without return from inactivation (model 7) was ranked near the bottom of the models tested by Akaike's asymptotic information criterion ranking. The constraints on the rate constants produced unacceptable results with the single-channel data. Note that we were unable to test the complete Hodgkin-Huxley model with return from inactivation because it has eight states, which is beyond the range of our analysis.

Preferred single-channel model

The single-channel model (model 3) selected for further analysis is shown below:

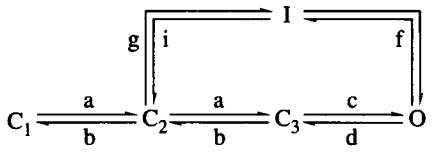

Model 3

Models 2 and 3 can be compared statistically to model 1 because they are nested subhypotheses. Likelihood ratios showed that models 2 and 3 were indistinguishable from model 1 ($P = 0.16$ and $P = 0.15$; Table 2), indicating that the additional inactivation pathways present in model 1 did not make it a statistically better model. Akaiki's Information Criterion (AIC) also ranked models 2 and 3 above model 1 (Table 1). Model 2 cannot be compared statistically to model 3 because neither is a subhypothesis of the other. Their relative log(likelihood)'s are nearly identical (Table 1), but because model 2 has one fewer free parameters, its AIC ranking is higher than model 3. Of these nearly equivalent models, model 3, with inactivation from both open and closed states, was selected for further analysis over the more parsimonious model 2, with inactivation only from the closed state C_3, because model 3 is more compatible with gating current data. Model 3 has the ability to be easily expanded to accommodate a series of inactivated states parallel to the activation pathways, a feature which will be used later in the extended model (below) to explain the fast OFF gating charge that is not immobilized by inactivation (Armstrong and Bezanilla, 1977; Nonner, 1980; Keynes, 1986).

Rate constants estimated for model 3, together with their standard errors, are shown in Fig. 2. Forward rates *a* and *c* along the activation pathway were voltage dependent, increasing with depolarization, and reverse rates *b* and *d* were voltage dependent in the opposite direction, increasing with hyperpolarization. The fitted lines indicate that the rates are an exponential function of voltage within the voltage range examined of −58 to −28 mV. Rates *g* and *f* of inactivation from the closed and open states were low compared to the activation and deactivation rates. The voltage dependence of inactivation exhibited a large degree of uncertainty due to the scatter in the estimated rates and their large standard errors, particularly at the most negative voltage examined. The best fits to the data indicate voltage dependences equivalent to 0.5–0.6 charges traversing the membrane field. The inactivation rates estimated for pulses to −58 mV have a great deal of uncertainty because the channels tend to close rather than inactivate at this negative potential (note the large error bars for *g* and *f* in Fig. 2). When only the more reliable estimates from −48 to −28 mV are considered, voltage dependences as low as 0.1 charges also could provide a good fit to the data.

The voltage dependences and magnitudes of the rates shown for model 3 were similar to those obtained from the other models, but the magnitudes of the inactivation rates varied depending on the number of inactivating pathways. Inactivation rates were faster when there were fewer allowed paths for inactivation, to maintain the overall rate of inactivation, and inactivation from closed states was more rapid than inactivation from the open state.

As with many investigations of single-channel kinetics, the analysis was limited by the bandwidth of the recordings. Even in physiological sodium concentrations (~500 nM) in the absence of extracellular divalents, the amplitude of single sodium channel currents was small (Correa et al., 1991; Vandenberg and Bezanilla, 1991). Recordings were made at 5°C to improve the current resolution, because lowering the temperature slowed the channel kinetics more than it decreased the current

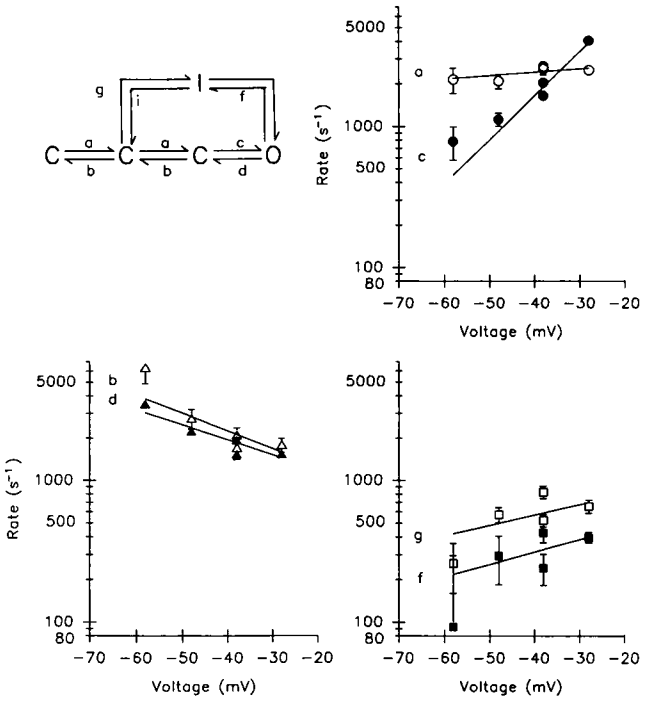

FIGURE 2 Rates for the preferred single-channel model. The preferred model (*upper left*), selected from models with five or fewer states, permitted transitions to the inactivated state (I) from one of the closed states (C_2) as well as the open states (O). The symbols represent the estimated rate constants. Standard errors are shown except when they are smaller than the symbol size. Lines show fits to the estimated rate constants, assuming that they are exponential functions of voltage. Data were fitted using weighted least squares, with the weighting factor equal to the inverse of the estimated variances. Fitted parameters yield charges and zero voltage rates of: rate a, 0.13 e^-, 2969 s^{-1}; rate b − 0.70 e^-, 704 s^{-1}; rate c, 1.25 e^-, 28932 s^{-1}; rate d, −0.60 e^-, 725 s^{-1}; rate f, 0.49 e^-, 705 s^{-1}; rate g, 0.66 e^-, 1,117 s^{-1}. The sum of the reverse rates from the inactivated state (rate i and rate I to O) had a total of 20–25 s^{-1} throughout the voltage range, however the uncertainties in these rates was too large to determine the voltage dependences of the return rates.

amplitude. It was possible to use a bandwidth of 3.1 KHz during the analysis without introducing spurious transitions due to the baseline noise. However, we estimate that channel dwell times <50 μs were missed due to filtering. Comparison of models was performed in the absence of missed-event correction because such corrections caused a large increase in computational time (>24 h/data set), large uncertainty in the estimated parameters, and often an inability for the minimization routine to converge on a solution. The final single-channel model (model 3) was analyzed extensively applying correction for missed-events of 10, 25, and 50 μs (Roux and Sauve, 1985). The absolute values of the rates were increased, but the voltage dependences of the rate constants were changed little. The rates reported here are without missed event correction because it was not possible to obtain reliable estimates at the most negative potentials using missed event correction.

Single-channel density histograms and model predictions

Histograms of single-channel properties are shown in Figs. 3–5 together with predicted probability densities based on the estimated rate constants for model 3 (Fig. 2). The histograms predicted from the rate constants show excellent agreement with those derived from the single-channel data, indicating the strong predictive power of the model.

The first latency densities (Fig. 3) show that as the potential was made more depolarized, the channel reached the open state for the first time more rapidly. At negative potentials, the time to first opening was broadly distributed in time, and the mean time was slower than at more positive potentials.

Once the channel opened, it reopened several times before it inactivated. Fig. 4 shows the number of openings per record together with predictions from the estimated rate constants. At a negative potential of −58 mV the mean number of openings per record was 0.7, whereas this number increased to 3.7 at −28 mV. If blank records are not considered, the mean number of

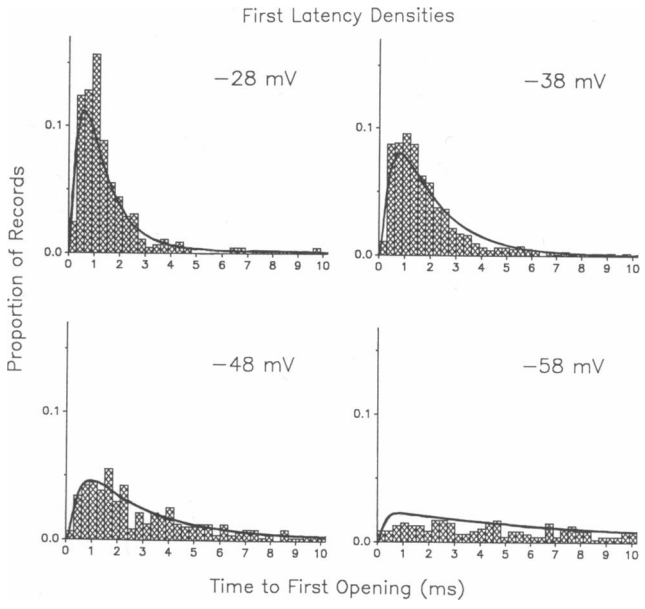

FIGURE 3 Comparison of first latency densities for one-channel patch with model predictions. Time to the first opening during voltage pulses to −58, −48, −38, and −28 mV (*hatched bars*), are shown with predicted first latency density (*solid line*) obtained using rate constants from the single-channel model (Fig. 2).

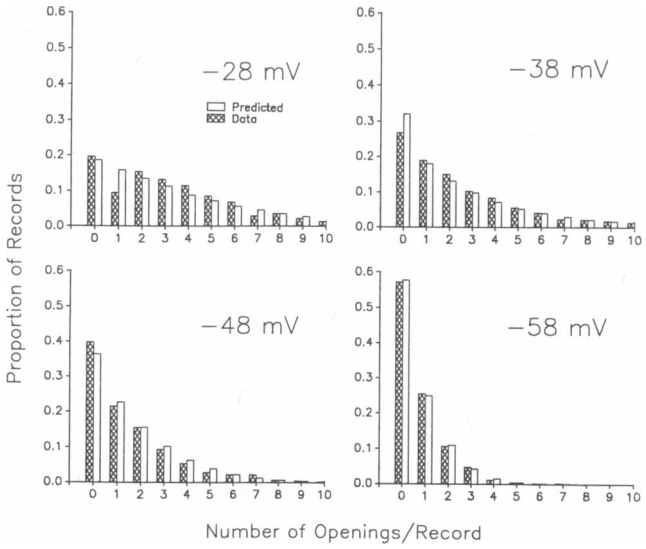

FIGURE 4 Comparison of number of openings per record with model predictions. Number of openings were tabulated for 22-ms pulses to −58, −48, −38, and −28 mV (*hatched bars*), and are shown with predicted number of openings per record (*open bars*) obtained by simulation using rate constants from the single-channel model (Fig. 2).

openings per record with at least one opening is 1.6 at −58 mV and 4.6 at −28 mV. Because the duration of a record was fixed at 22 ms, and channels may return slowly from the inactivated state, it is useful to compare the number of openings expected in 22 ms with the number of openings before a channel reaches the inactivated state, which we term a burst of openings. The number of openings per burst predicted from the rate constants is 2.1 at −58 mV, whereas this number nearly doubles to 3.7 at −28 mV. Throughout this range the average duration of a burst was fairly constant at 4.5–4.6 ms. Thus, at −58 mV only ~75% of the openings from the first burst of openings had occurred by the end of the 22-ms record, but at −28 mV, the channel had inactivated and ~25% of the openings resulted from a second burst of openings after the channel returned from inactivation.

The open and closed time histograms, and their predicted densities are shown together in Fig. 5. The open time histogram was well described by a single exponential which was the inverse of the sum of the rate constants d and f estimated from the model, thus providing evidence for one open state in this potential range. The closed time density was a more complicated function based on the dwell times of the channel in the various closed states before reopening, and also was well fit by the model. The mean open time increased slightly with depolarization, whereas the mean closed time decreased with depolarization (Fig. 6). Thus, during a burst of openings at positive potentials, the proportion of time the channel was open was higher than at negative potentials due to both an increase in mean open time and a decrease in mean closed time.

Whereas the preferred single-channel model showed excellent prediction of gating parameters that rely on transitions near the open state (open time, closed time, number of openings per record), it would not be expected to accurately predict the ON gating currents which primarily reflect charge movement among closed states far from the open state. Indeed, gating currents predicted from single-channel models showed a rising phase as has been previously described (Vandenberg and Horn, 1984). The single-channel models were unable to incorporate the larger number of closed states that previous studies have shown were required to fit the gating currents (Stimers et al., 1987). Single-channel maximum likelihood analysis indicated that additional closed states would improve the model, but insufficient information was available from single-channel data alone to estimate the transition rates.

Expanded gating model

Maximum likelihood analysis of single-channel data provided a statistical basis for comparing kinetic models and selecting a model that well described the transitions near the open state. That model then was used as the basis of an expanded characterization of the channel kinetics incorporating gating current and macroscopic ionic current measurements over a wider voltage range. Single-channel first-latency densities also were included in the expanded modeling. This allowed the formulation of a model that was compatible with single-channel measurements, and also was able to describe the charge movements associated with ON and OFF gating currents and ionic activation and tail currents. The scope of the voltage range was extended to encompass activation pulses between −50 and +2 mV and tail pulses from −98 to −28 mV.

The expanded model,

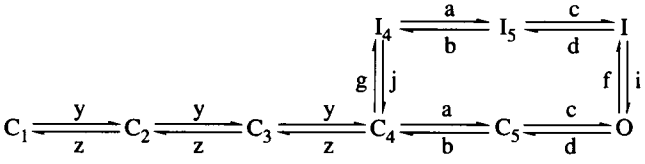

incorporated a minimum number of changes from the single-channel model while providing good agreement with patch macroscopic ionic (Fig. 7) and gating (Fig. 8) currents. The first latency densities, obtained as average first-latency densities from three one-channel patches, also were well described by the rate constants (Fig. 9).

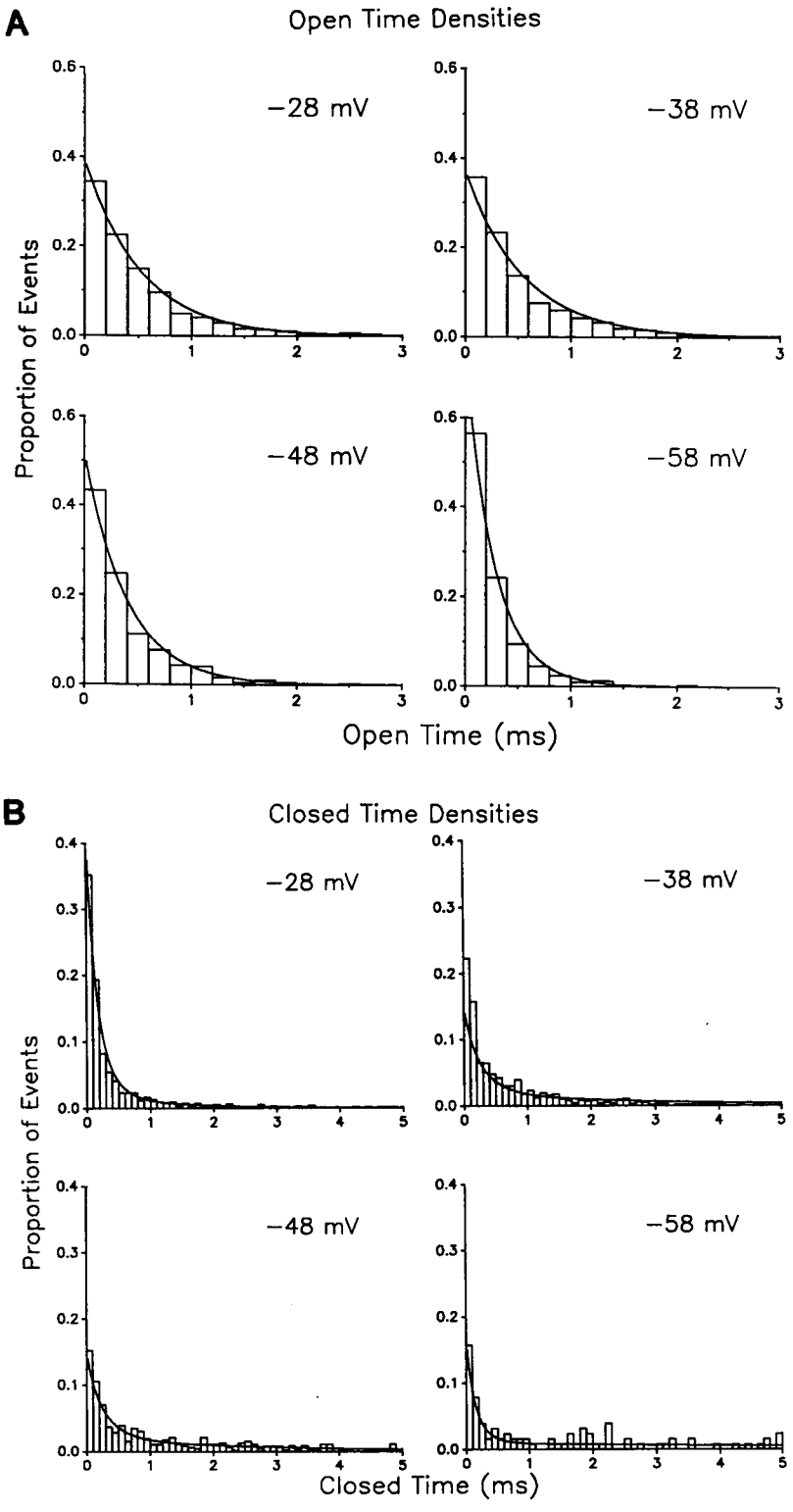

FIGURE 5 Comparison of open and closed time densities with model predictions. (*A*) Open time histograms, and (*B*) closed time histograms for 474 pulses each to −58, −48, −38, and −28 mV. Data in the closed time histogram include only times between channel openings, and do not include time to first opening or time after the last opening in the record. Predicted open and closed time densities (*solid lines*) were obtained using rate constants from the single-channel model (Fig. 2).

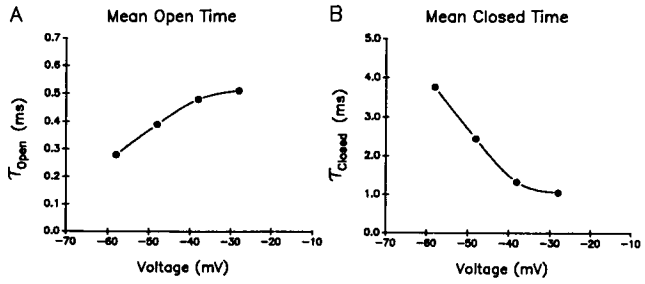

FIGURE 6 Mean open and closed times versus voltage. For details see text.

All these data were simultaneously fitted over the entire voltage range assuming that the rates were simple exponential functions of voltage (see Methods). A summary of the equations used to describe the expanded model, including the zero-voltage rate constants, gating charges and fractional electrical distance of the energy barriers is presented in Table 3.

The simplest model that was compatible with gating and ionic current data required nine states arranged as shown. Two additional closed states were needed at the beginning of the activation pathway to fit the ON gating current without a rising phase (Fig. 8 *A*). OFF gating currents (Fig. 8 *B*) necessitated a further addition of inactivated states to the model to account quantitatively for the amount of fast charge movement when the membrane was repolarized. To minimize the number of free parameters introduced with the expanded model, the interactions between the parallel set of inactivated states I_4, I_5 and I were assumed to be equal to those between the states C_4, C_5 and O, and their rates were made identical.

The rates between the first four closed states C_1, C_2, C_3, and C_4 were made equal to each other based on comparison with two types of alternative models that had similarity to the Hodgkin and Huxley (1952) independent gating particle model. In the first alternative model, the first three forward rates were $3y$, $2y$, y, and the backward rates were z, $2z$, $3z$. Models of this type were not able to simultaneously fit gating and ionic currents. In particular the initial phase of the gating current was too fast, and later phases too slow when there was a good fit to ionic current (data not shown). In the second alternative model, the relationship between the closed states was made more flexible, and the rates were allowed to vary by a fitted factor u from each other:

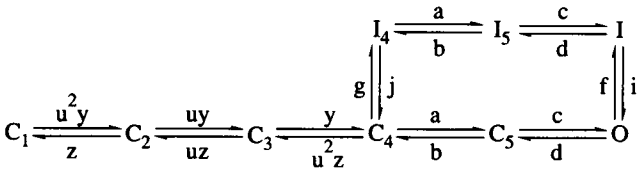

The best fit was obtained when u was 1.1, and was essentially unchanged when u was equal to 1.0 (the error function was increased $<0.04\%$). On that basis in the extended model the first three forward rates from states C_1 to C_4 were made equal to each other (rate y in the

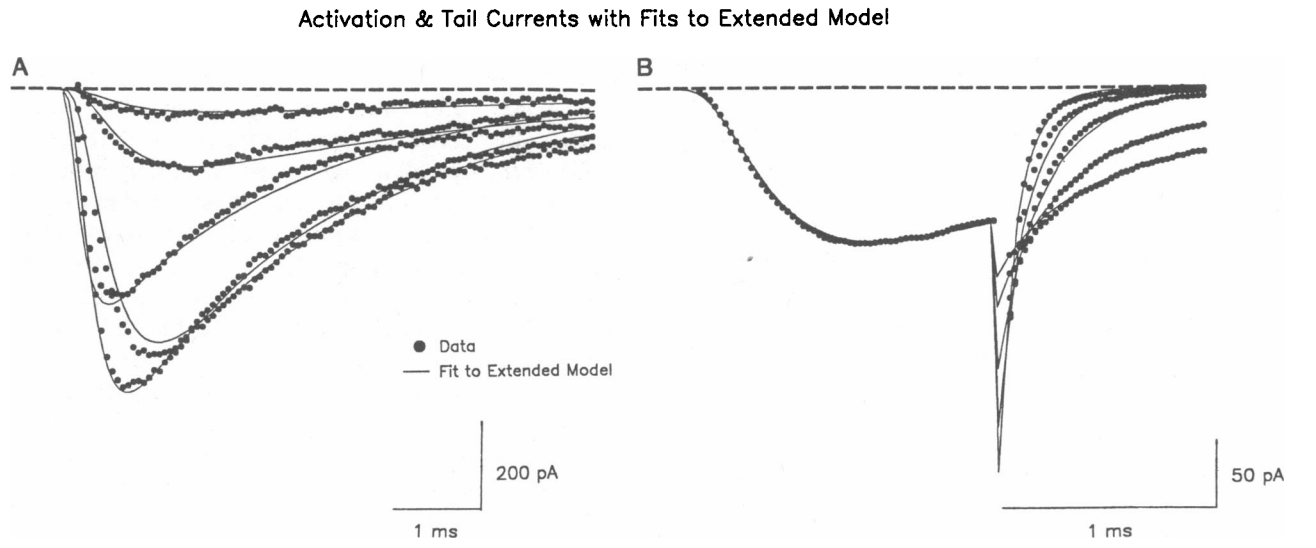

FIGURE 7 Macroscopic ionic currents fitted with extended model. Results are shown for simultaneous fitting for families of macroscopic activation and tail currents. (*A*) Records for ionic current are for pulses to −48, −38, −18, and +2 mV from a holding potential of −108 mV. (B) Ionic tail currents are for postpulses to −98, −78, −58, −38, and −28 mV following a 1.5 ms pulse to −8 mV from a holding potential of −108 mV. Currents represent averages of 16 cycles.

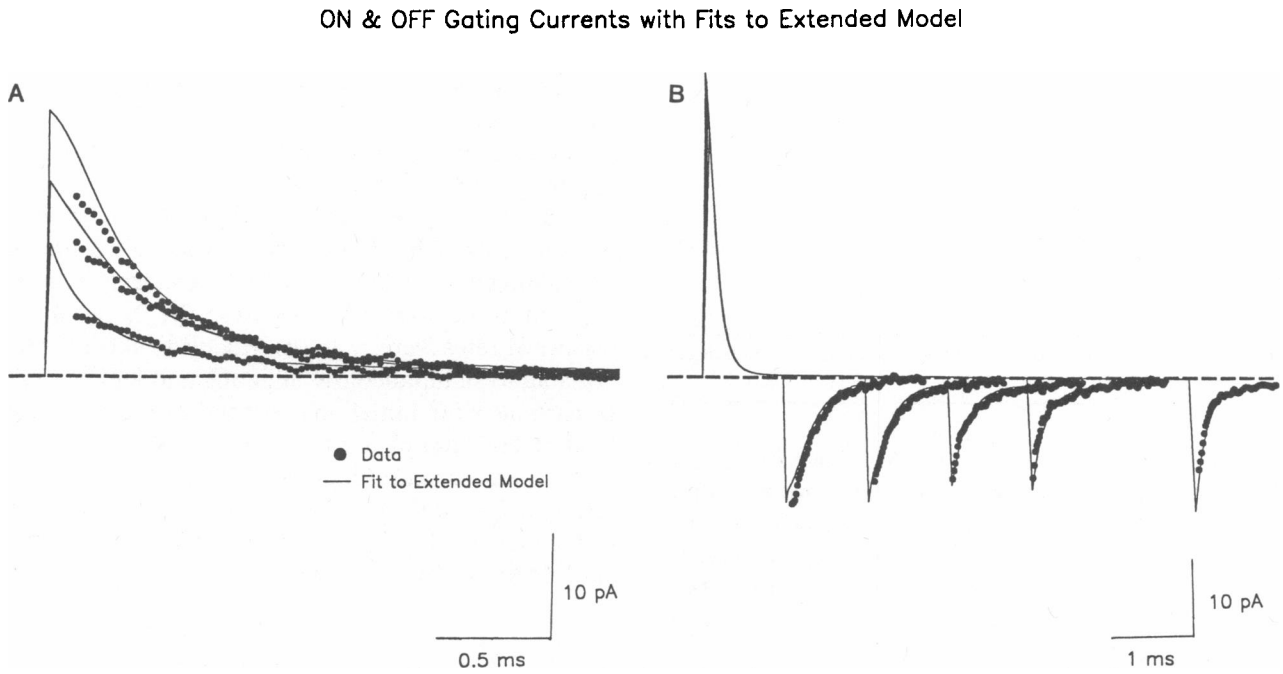

FIGURE 8 ON and OFF gating currents fitted with extended model. (*A*) ON gating currents are fitted during 2.7-ms pulses to −50, −30, and −10 mV from a prepulse potential of −110 mV. (*B*) OFF gating currents are for postpulses to −95 mV following a variable-duration (1, 2, 3, 4, and 6 ms) pulse to +30 mV. Currents represent averages of 50–80 cycles; bandwidth 8 KHz. The first 125 μs of the data records (not shown) were not used in the fitting due to filtering.

diagram), and the corresponding three reverse rates made equal (rate z).

The rates derived from the extended model by chi-squared minimization (Fig. 10 and Table 3) were very similar to the rates from the single-channel maximum likelihood estimates (Fig. 6), particularly for rates c and d which were best estimated from single-channel data. As with the single-channel model, the forward rate constants y, a, and c increased with depolarization, whereas the reverse rates z, b, and d increased with hyperpolarization. The equivalent gating charges, derived from the sum of the voltage dependences for the forward and reverse rates, were 1.5 e^- for each of the three transitions between the closed states C_1, C_2, C_3 and C_4, and 0.4 e^- between states C_4 and C_5. The transition between the last closed state C_5 and the open state O carried the most charge, equivalent to 1.9 e^-. The rates, f for inactivating from the open state, and g for inactivating from the closed state C_4 were voltage independent for the best fit. Qualitatively acceptable fits could be obtained allowing voltage dependences up to 0.3 e^- for the inactivation rates. The return rate from the inactivated states were voltage dependent, however, producing an equivalent gating charge of 0.9 for the transition between states I_4 and C_4, and between states I and O.

Comparison of rate of return from inactivation with model predictions

A test of the quality of the model can be made by examining the predictive power of the model for data that were not included in the formulation of the model, and which represent a voltage range that was not specifically tested for those rates. Calculations were made of the overall rate of recovery from inactivation at various voltages (Fig. 11), and these predictions were compared to published rates of recovery from inactivation from perfused squid axons under axial wire voltage clamp (Bezanilla and Armstrong, 1977; Keynes, 1986). The published data were corrected for the effects of external divalents, junction potential, and temperature (see legend of Fig. 11). Fig. 11 shows very good agreement with the predicted curve using the estimated rates and voltage dependences from the extended model. The overall predicted rate of return from inactivation had a voltage dependence of 0.9 e^-, which is close to the value of 0.8 e^- reported by Keynes (1986).

Predictions from the extended model

The single-channel behavior underlying the macroscopic current can be deduced by examination of the voltage

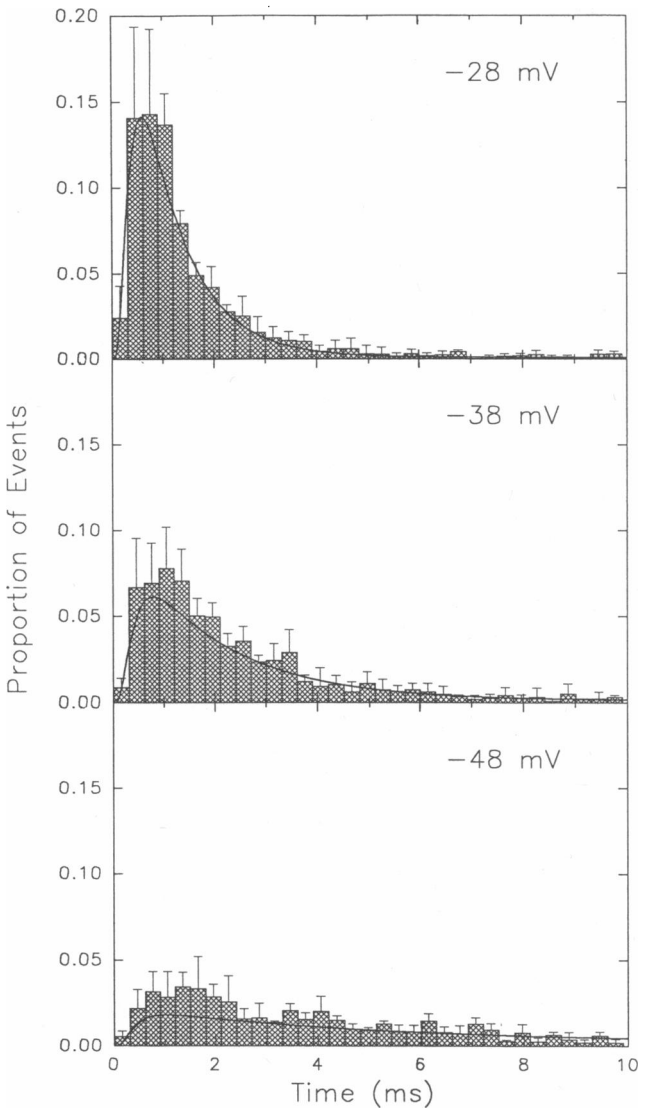

FIGURE 9 Average single-channel first latency densities fitted with extended model. The time to the first opening during voltage pulses to −48, −38, and −28 mV (*hatched bars*) were averaged from three one-channel patches. Results for each voltage were obtained from 1,600–1,750 single-channel current records (400–900 records/patch). The error bars represent standard deviations of the histograms measured from the three patches. The continuous line is the prediction from the extended model. The three one-channel patches appeared to be representative of the gating behavior of the channel population, and showed good agreement in channel open time (Fig. 12) and in average current (not shown)

dependence of the rate constants. Qualitatively different single-channel currents are predicted at different voltages depending on the dominant rates at each voltage. Important differences in kinetic properties appear at crossover voltages where the relative magnitude of rates changes.

For example, at very negative potentials (< -45 mV) the deactivation rate z exceeds the activation rate y. Individual channels may make progress from the closed state C_1 towards the open state O, but the overall rate is slow because at each step the channel is more likely to return to a previous closed state than move in the direction of the open state. The channel will probably inactivate from the closed state before it reaches the open state. If the channel does reach the open state, it does so after a long latency, and is likely to close rapidly and inactivate from the closed state. This behavior leads to a macroscopic current whose overall waveform is based on the long latency to channel opening, with little contribution from channel open time or channel reopening kinetics.

The fate of an open channel at negative potentials can be examined further by comparison of the extended model rates d and f for closing or inactivating from the open state, with the time course of macroscopic tail currents and the single-channel open time (Fig. 12). The closing rate d is similar to the tail current rate (*open symbols*) for potentials more negative than −50 mV, and the inverse of the mean channel open time (*filled symbols*). This shows the close agreement between single-channel and macroscopic measurements. It suggests that negative to −50 mV the channel closes and does not tend to reopen before inactivating. If reopenings were frequent, the tail current rate would be slower than the closing rate. A second small slow component in the tail current may be due in part to a very low probability of late reopenings. The closing rate d is much larger than the inactivating rate f, showing that channel closing along the deactivation pathway is the dominant fate of open channels in this voltage range. Our rates of inactivation are consistent with the results of Levis (1988) who showed that the channel open time was unchanged after inactivation was removed with pronase, suggesting that the inactivation rate from the open state is very low compared to the closing rate.

At most potentials in which the sodium channel is active (between −45 and +60 mV), the single-channel behavior reflects a combination of many rates. At these potentials, the channel shows bursting activity, as it closes and reopens several times before inactivating from either the closed or open state. Macroscopic ionic current results from a combination of first latency density and burst duration.

The probability of finding the channel in each of the states is shown in Fig. 13 for voltage pulses to −40 mV, −20 mV, and +10 mV. In all cases the channel tends to open several times before inactivating, suggesting that burst duration plays an important role in the macroscopic current. However, the contributions of the individual closed states varies considerably. At +10 mV, $< 10\%$ of the time is spent in the closed states after the peak

TABLE 3 Equations of the extended model

Differential equations for the state probabilities

$$\frac{dO}{dt} = cC_5 + iI - (d + f)O \qquad \frac{dI}{dt} = cI_5 + fO - (d + i)I$$

$$\frac{dI_5}{dt} = aI_4 + dI - (b + c)I_5 \qquad \frac{dI_4}{dt} = gC_4 + bI_5 - (j + a)I_4$$

$$\frac{dC_5}{dt} = aC_4 + dO - (b + c)C_5 \qquad \frac{dC_4}{dt} = yC_3 + bC_5 + jI_4 - (a + z + g)C_4$$

$$\frac{dC_3}{dt} = yC_2 + zC_4 - (y + z)C_3 \qquad \frac{dC_2}{dt} = yC_1 + zC_3 - (y + z)C_2$$

$$C_1 = 1 - (C_2 + C_3 + C_4 + C_5 + O + I_4 + I_5 + I)$$

Rate definitions

$$y = 16{,}609 \cdot \exp\left(1.50\,\frac{0.22 \cdot V}{24}\right) \qquad z = 971 \cdot \exp\left(-1.50\,\frac{0.78 \cdot V}{24}\right)$$

$$a = 5{,}750 \cdot \exp\left(0.42\,\frac{0.99 \cdot V}{24}\right) \qquad b = 4{,}325 \cdot \exp\left(-0.42\,\frac{0.01 \cdot V}{24}\right)$$

$$c = 15{,}669 \cdot \exp\left(1.91\,\frac{0.75 \cdot V}{24}\right) \qquad d = 1{,}361 \cdot \exp\left(-1.91\,\frac{0.25 \cdot V}{24}\right)$$

$$f = 432 \cdot \exp\left(0.91\,\frac{0.001 \cdot V}{24}\right) \qquad i = 4 \cdot \exp\left(-0.91\,\frac{0.999 \cdot V}{24}\right)$$

$$g = 770 \cdot \exp\left(0.91\,\frac{0.001 \cdot V}{24}\right) \qquad j = \frac{g \cdot i}{f}$$

Ensemble ionic current per channel

$$i_{Na} = \gamma_{Na} \cdot V \cdot \frac{\exp\left[(V - V_{Na})/24\right] - 1}{\exp\left(V/24\right) - 1} \cdot O$$

Ensemble gating current per channel

$$i_g = 1.6 \cdot 10^{-19}\{1.50 \cdot [y \cdot (C_1 + C_2 + C_3) - z \cdot (C_2 + C_3 + C_4)] + 0.42 \cdot (aC_4 - bC_5) + 1.91 \cdot (cC_5 + cI_5 - dO - dI) + 0.91 \cdot (fO + gC_4 - iI - jI_4)\}$$

V is membrane potential in mV; t is time in seconds, C_1 through C_5 and I, I_4 and I_5 are the probabilities of being in the corresponding states as defined in the kinetic diagram. γ_{Na} is the limiting single channel conductance (i.e., 35 pS), V_{Na} is the sodium reversal potential (i.e., 67 mV), and 24 is the value of RT/F at 5°C.

current has been reached. Bursts represent extremely rapid transitions to the closed states C_5 and C_4 before reopening. At −20 mV, considerably more time is spent in closed states C_5, C_4, and C_3. The probability of finding the channel in one of the closed states is equal to the probability of finding it in the open state throughout the inactivating phase of the macroscopic current. At −40 mV, all of the closed states are more populated than the open state throughout the voltage pulse. Even after 3 ms, when most of the channels have reached the open state for the first time, the probability of finding a channel in the first closed state C_1 is still higher than finding it in the open state.

DISCUSSION

Strategy for model development

The kinetics of sodium channel gating have been extensively studied. However, a model that can account for the kinetics of gating currents, single-channel ionic currents, and macroscopic ionic currents had not been developed previously due to the inability to measure all of these currents in the same preparation. We present here a study from the squid giant axon in which these currents were measured with patch techniques under similar conditions, and data were combined to develop a model of channel gating.

Different manifestations of sodium channel gating reflect different aspects of the gating process. Sodium single-channel currents are exquisitely sensitive to the rates governing channel closing-to-reopening transitions because, over the potential range in which they can be resolved, the dominant form of gating is a short burst of openings. Single-channel currents thus provide a good data set for comparing models and defining the relationship between states that are near the open state. We followed the maximum likelihood approach of Horn and Lange (1983) and Horn and Vandenberg (1984) to statistically compare models. Maximum likelihood anal-

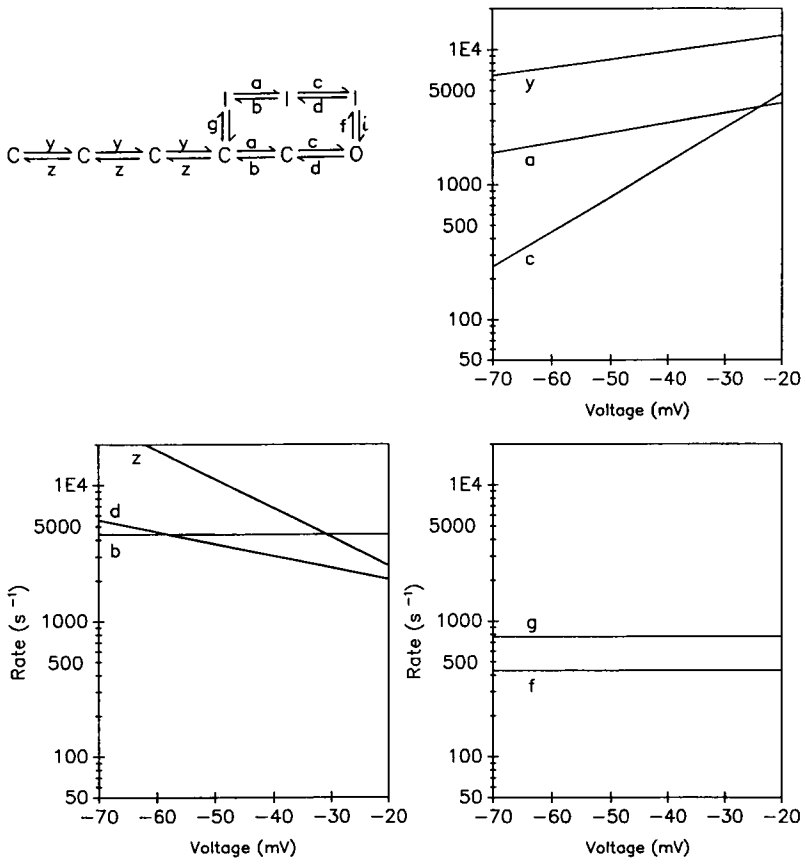

FIGURE 10 Rates for the extended model. Rates were derived from simultaneously fitting the macroscopic ionic currents (Fig. 7), the ON and OFF gating currents (Fig. 8), and the first latency density from single channel measurements (Fig. 9). The model is shown in the upper left panel. Activation forward rate constants are shown (*upper right*), deactivation backward rate constants (*lower left*), and inactivation rates (*lower right*). Voltage dependencies and zero-voltage rates are listed in Table 3.

ysis of single-channel currents also is able to point in the direction of expanded gating models, but insufficient information in the single-channel records limits the estimation of rate constants to smaller models.

Gating currents, in contrast provide information on fast voltage-dependent transitions between both closed and open states, and predominantly reflect the transitions that occur immediately after the voltage pulse. By analyzing ON gating currents, and OFF gating currents at various times during a voltage pulse, relationships among both early closed states and late inactivated states can be ascertained. Gating currents also permit a quantitative analysis of charge movement and charge immobilization during inactivation by requiring that the model simultaneously fit the ionic current from which the overall rate of inactivation can be ascertained. Macroscopic ionic currents further constrain the models throughout a wide voltage range. Ionic tail currents in combination with OFF gating currents are particularly instructive in estimating deactivation rates near the open state.

The approach which we used was to select a preferred model that could account for transitions near the open state by using the single-channel data and statistical criteria based on likelihood ratios and Akaike's asymptotic information criterion for ranking. That model was then expanded to the minimum extent to obtain agreement with gating and macroscopic ionic currents. The result is the simplest model that could quantitatively account for sodium channel gating.

Because different types of data represent different aspects of channel gating, the extent to which each type of data is weighted affects the final model. We chose to analyze an equal number of data records from each type, and weight the data points by their amplitude by minimizing the chi-squared deviation between the data and model prediction. In the absence of a compelling reason to select data, this provided a method to balance

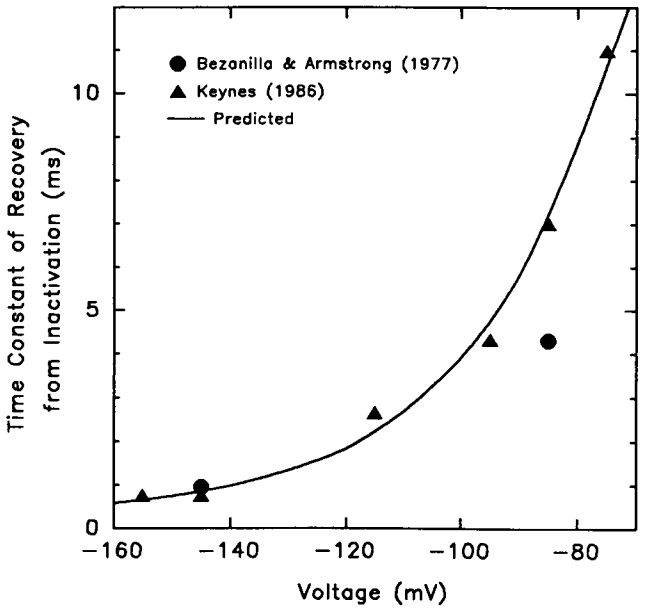

FIGURE 11 Predicted voltage dependence of rate of recovery from inactivation. The rate of recovery from inactivation was obtained at various voltages using the extended model by simulating the probability of finding the channels in all the inactivated states $I_{tot}(=I_4 + I_5 + I)$ as a function of time following a 10-ms pulse to +10 mV that caused 98% of the channels to inactivate. The time course of decline of I_{tot} was nearly exponential, and the time constant is plotted together with data reported by Bezanilla and Armstrong (1977; *filled circles*) and Keynes (1986; *filled triangles*). The data were shifted by 15 mV to hyperpolarized potentials to account for the effects of external divalent cations (12 mV) and junction potential (3 mV; Vandenberg and Bezanilla, 1991). The data of Bezanilla and Armstrong (1977) also were corrected for differences in temperature from 8 to 5°C using a Q_{10} of 2.5.

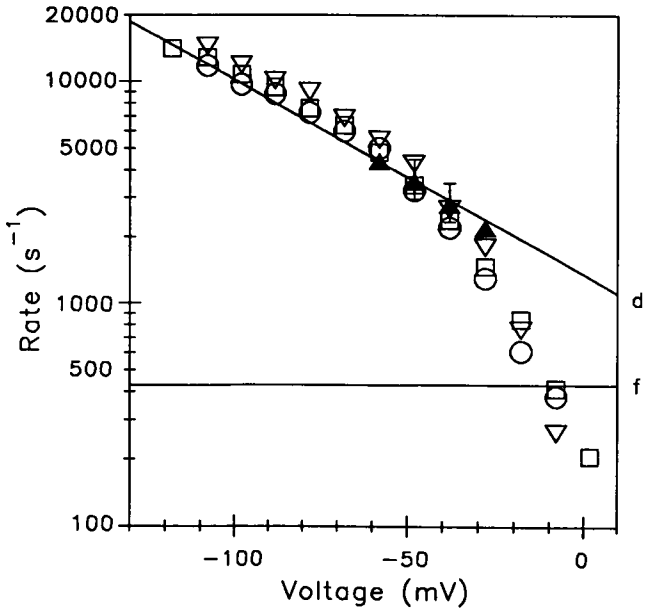

FIGURE 12 Comparison of tail current, deactivation and inactivation rates, and mean open time. Single exponential fits to tail currents elicited following an activating pulse to −8 mV (*open symbols*), are shown together with the inverse of the mean channel open time (*filled triangles*). Mean open time was obtained by maximum likelihood estimation (Vandenberg and Horn, 1984) using a missed event correction of 50 μs. Mean open times are the average of open times from 1–3 one-channel patches, and error bars represent standard deviation. Rates *d* and *f* from the extended model (Fig. 10) for closing or inactivating from the open state, respectively, are plotted with solid lines.

the types of data and correct for differences in the magnitude of the records.

Exponential voltage dependence of transition rates

An assumption used in fitting the data with the extended model is the exponential dependence of the rate constants over the voltage range studied, from −98 to +2 mV. The exponential dependence represents a first approximation at a low field strength of the rates of protein conformational changes including fixed-charge and dipole interactions (Stevens, 1978). This approximation was important in reducing the number of free parameters in fitting the data for the extended model, and is supported by the exponential dependence of the estimated rate constants from single-channel analysis Fig. 2) in the voltage range −58 to −28 mV.

A model of sodium channel gating

The extended model of sodium channel gating incorporates aspects of models developed by Hodgkin and Huxley (1952), Bezanilla and Armstrong (1977), Armstrong and Bezanilla (1977), Armstrong and Gilly (1979), and Stimers et al. (1985) to describe ionic and gating currents in the squid giant axon, and is similar to the model developed by Horn and Vandenberg (1984) for GH_3 cells. The distinguishing features of the model are: (*a*) a long series of closed states are required in the

FIGURE 13 Model of channel behavior at various voltages. With the rates derived from the extended model, the probabilities of finding the channel in each of the closed states, the open state, and the inactivated states were calculated during voltage pulses to −40, −10, and +20 mV from a holding potential of −108 mV. Probabilities are shown for the open state (*solid line*), closed state C_1 (*dotted line*), C_2 (*short dashes*), C_3 (*medium dashes*), C_4 (*long dashes*), C_5 (*dash-dot*), and the sum of all three inactivated states I_{tot} (*dash-dot-dot*).

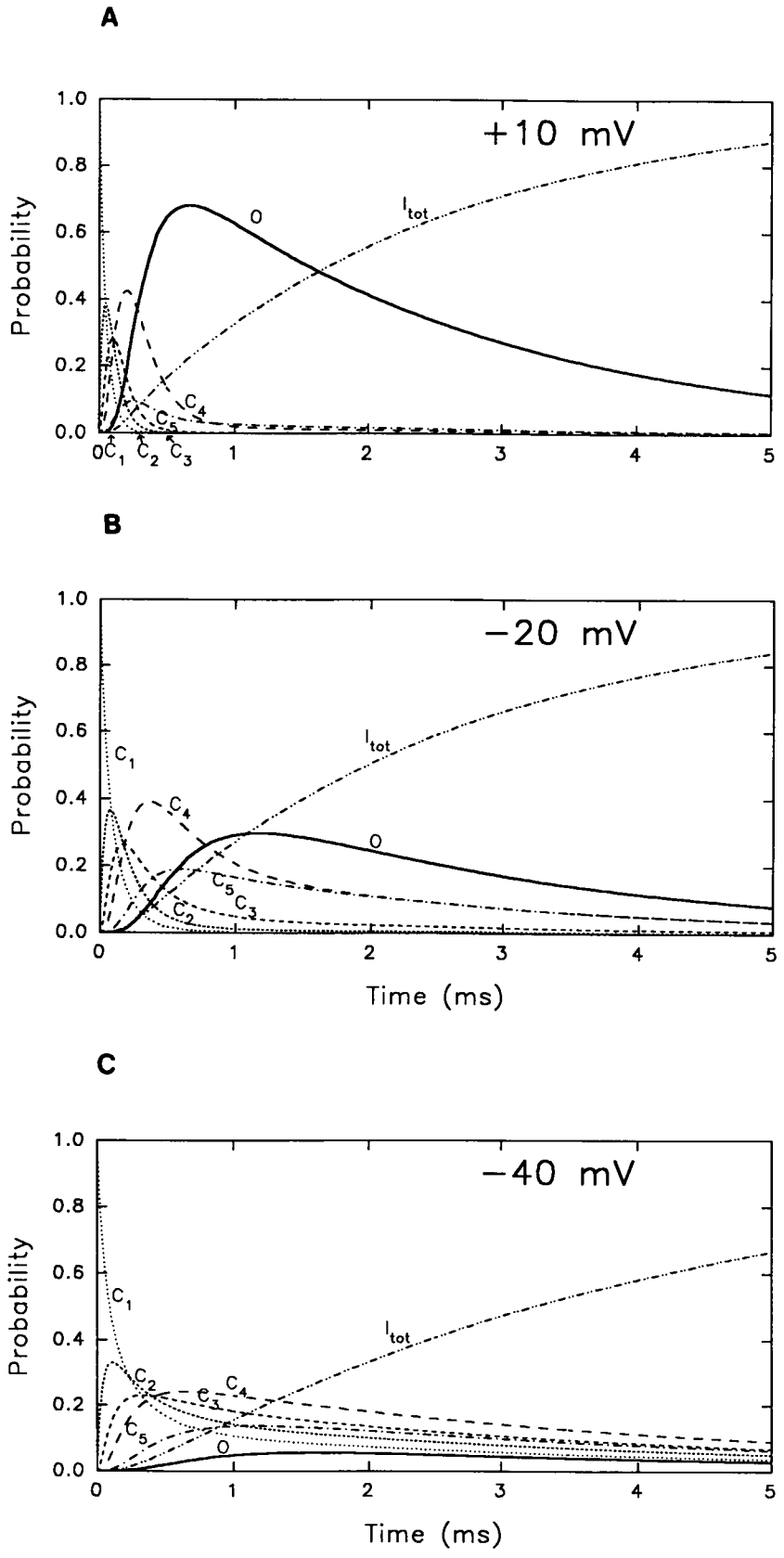
A
+10 mV
Probability
1.0
0.8
0.6
0.4
0.2
0.0
O
I_{tot}
C_4
C_5
C_1
C_2
C_3
0
1
2
3
4
5
B
−20 mV
Probability
C_1
I_{tot}
C_4
O
C_5
C_3
C_2
Time (ms)
C
−40 mV
Probability
C_1
I_{tot}
C_2
C_4
C_3
C_5
O
Time (ms)

activation pathway, (*b*) a set of inactivation states are found in parallel to the activation states, (*c*) channels inactivate from open and closed states, (*d*) inactivation is reversible, (*e*) the rate constants are not constrained by the independent gating particle hypothesis for 3 or 4 m activation gates and 1 h inactivation gate, and (*f*) several of the possible transitions between states are not required.

The model allows activation and deactivation to proceed along the same pathway. This is in agreement with the work of Oxford (1981), in which he examined the effects of interrupting a depolarizing pulse by a brief hyperpolarizing pulse of varying duration before reinitiating the depolarizing pulse. His observation of monoexponential kinetics of reactivation for brief duration hyperpolarizing pulses is consistent with a single pathway for activation and deactivation of the channel. This type of model was sufficient to explain the data presented here, and we did not examine more complicated schemes such as the parallel activation and deactivation pathways that were proposed by Alicata et al. (1990) to explain D_2O effects on channel gating.

The present model has one open state. Our observation of a mono-exponential open time density is consistent with a single open state, as are the majority of open times reported from a variety of preparations (e.g., Horn and Vandenberg, 1984; Patlak and Ortiz, 1986; Scanley et al., 1990), although occasional biexponential distributions of sodium channel open time have been reported (Nagy, 1987). Recent single-channel studies in the squid axon with steep sodium gradient and reverse sodium gradient indicate that the channel may adopt a second open conformation at very positive potentials (Correa and Bezanilla, 1990; Bezanilla and Correa, 1991), in agreement with previous macroscopic current studies for positive potentials (Bezanilla and Armstrong, 1977; Armstrong and Bezanilla, 1977). This second open state is observed at potentials beyond the range of this study, and will be the basis for extending the model to more positive potentials.

Immobilization of gating charge

OFF gating charge is partially immobilized during a depolarizing pulse with the same time course as inactivation of the ionic current (Armstrong and Bezanilla, 1977; Nonner, 1980; Keynes, 1986). The immobilized gating charge has a slow rate of return from inactivation, and can be seen in OFF gating currents as a slow component of the current whose rate increases as the postpulse is made more negative (Armstrong and Bezanilla, 1977; Keynes, 1986). Armstrong and Bezanilla (1977) and Stimers et al. (1985) proposed that an interaction exists between the activation gating particles and the inactivation gating particles that would slow the return from inactivation. Stimers et al. (1985) allowed channels to deactivate rapidly between the three inactivated states nearest the open state to account for the approximately one third of the gating charge that is not immobilized by inactivation, but return from any of those three states to other states would be slow to describe the slow return of immobilized charge. Our model is similar to the model of Stimers et al. (1985) in the arrangements of states and the existence of charge movement among inactivated states near the open state. The presence of only three parallel inactivated states near the open state has the same effect as an interaction between activation and inactivation gating particles, although to simplify the model we do not formally invoke such an interaction in our description of rate constants.

Voltage dependence of activation and deactivation rates

The equivalent gating charge for opening the channel from rest was 6.8 e^-, obtained by summing the charges for each of the six state transitions from C_1 through O. This value is much greater than the estimate of 3 e^- obtained from measuring the slope of the peak fraction of channels open vs. voltage curve at negative potentials (Vandenberg and Bezanilla; 1991). This is consistent with the observation that estimates of activation gating charge derived from conductance measured at the peak current in the presence of channel inactivation are underestimated significantly due to inactivation of the channel (Stimers et al., 1985).

Voltage dependence of inactivation

The questions of the inherent voltage dependence of inactivation of sodium channels, and the degree of coupling to the activation process have generated considerable controversy. In the squid, where macroscopic inactivation rates are relatively less voltage dependent than in mammalian cells, a low degree of voltage dependence has been assigned to the inactivation rate. We find that a voltage dependence equivalent to 0–0.3 e^- best fits the inactivation rates from the open and closed states, whereas the return rates have a voltage dependence of 0.9 e^-, giving an equivalent gating charge for the overall transition of 0.9–1.2 e^- the majority of which derives from the voltage dependence of return from inactivation. Stimers et al. (1985) argued that a modest voltage dependence (0.6 e^-) of the inactivation rate was required to achieve saturation of the peak fraction of channels open vs. voltage curve. Indeed, the

predicted peak *F–V* curves from our extended model do not saturate until positive potentials, but the expected increase in the peak *F–V* curve at positive potentials is small (81% open at +40 mV, increasing to 91% open at +100 mV). Such a small increase would not be easily detected because the conductance in this voltage range is derived by dividing two very small numbers. In frog muscle, Nonner (1980) proposed that some small voltage dependence should be assigned to inactivation itself to predict the small voltage dependence of macroscopic inactivation at large depolarizations.

Single-channel studies have been used to estimate the voltage dependence of inactivation, and in other preparations have suggested values that vary between 0 and 1.9 e^- with most values between 0 and 1 e^-: 0.1-0.5 e^- in neuroblastoma cells (Aldrich et al., 1983; Aldrich and Stevens, 1987), 0.9 e^- in cardiac cells (Scanley et al., 1990), in GH_3 cells 0.7 e^- (Horn et al., 1984) or 1.9 e^- with a decrease at positive potentials (Vandenberg and Horn, 1984). The single-channel analysis presented here shows voltage dependence of the inactivation rates in the range of 0.1–0.6 e^-, which is in agreement with the estimates derived from the extended model of 0.0–0.3 e^-.

The difference in voltage dependences of inactivation and return from inactivation suggests that the activation energy barrier for this transition is very asymmetric with respect to the membrane field. It also shows that most of the voltage dependence of the inactivating phase of macroscopic sodium currents in the squid is not due to an inherent voltage dependence of the inactivation rate. The rate of macroscopic inactivation largely is due to a combination of rates for transitions between states associated with activation, deactivation and inactivation pathways. Because the activation and deactivation state transitions are voltage dependent, the macroscopic rate of inactivation derives voltage dependence due to its partial coupling to the activation/deactivation process. However, inactivation is not strictly coupled to channel opening. Closed channels as well as open channels inactivate, with the relative proportion of channels following the different inactivation pathways determined by the membrane potential.

These results predict that there will be a component of gating current due to inactivation that would be removed if inactivation were eliminated. Because the forward inactivation rates are not very voltage dependent, the rate of this component of ON gating current will depend on the partial coupling of inactivation with activation. Inactivation gating current will be very low in amplitude and slow because the inactivation rate is slow and occurs late in the activation scheme. Simulations of predicted gating and ionic current with and without inactivation (Fig. 14) indicate that squid inactivation gating current will be almost indistinguishable during the slow tail of ON gating current similar to that predicted by Vandenberg and Horn (1984) for mammalian cells. A small slow component of gating current correlated with inactivation has recently been reported in the squid (Bekkers et al., 1990; see also Swenson, 1983, for crayfish).

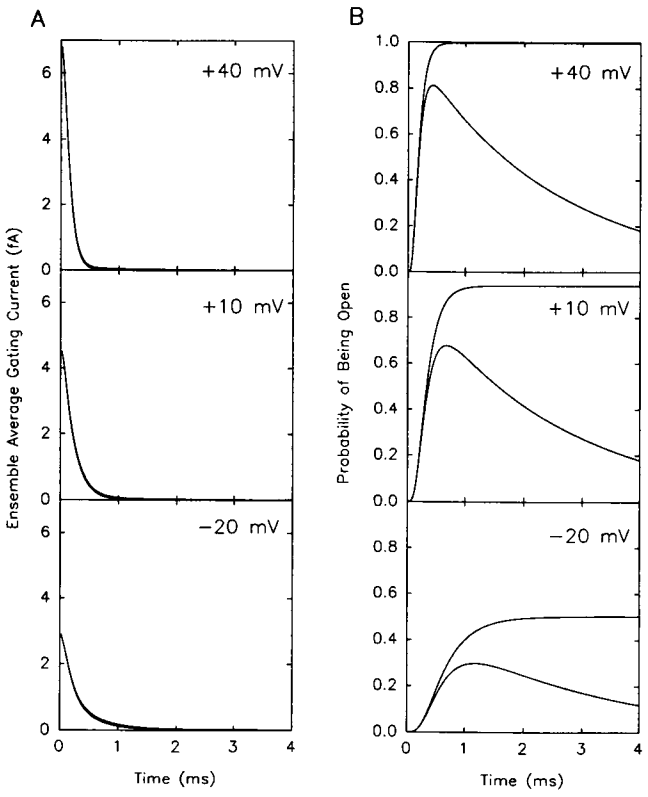

FIGURE 14 Predicted ensemble average gating currents and ionic currents with and without inactivation. (*A*) Ensemble average gating currents and (*B*) probability of a channel being open were simulated with the extended model for 5-ms voltage pulses to +10, −20, and −40 mV, from a holding potential of −98 mV. Simulations in the absence of inactivation were obtained by setting the inactivation rates *g* and *f* to zero, resulting in the lower curves in gating current (*A*), and the upper curves in probability of being open (*B*).

Gating particles are not both independent and identical

With the availability of sequence information for the alpha subunit of several sodium channels (Noda et al., 1986), one can ask how kinetic modeling information can be reconciled with proposed structural models. Purified sodium channel from a variety of sources have a similar alpha subunit of 260–290 kD, which in mammalian brain and skeletal muscle are found associated with smaller beta subunit(s) (Catterall; 1986). Sequence data for the alpha subunit cDNAs from several sources show

four homologous domains, each with six or eight proposed membrane spanning regions (Noda et al., 1984; Guy and Seetharamulu, 1986). One of these, the putative amphipathic helix S4, has been proposed to form a part of the voltage sensor (Noda et al., 1984). A high degree of homology exists among the sequences of sodium channels from *Drosophila* to rat brain (see Salkoff et al., 1987). Although the amino acid sequence and subunit composition of the squid sodium channel are not yet known, one could expect a similar general arrangement to that found for other sodium channels.

If the homologous domains function identically and independently as voltage sensor/gating particles, channel gating kinetics would be described by a model similar to the Hodgkin-Huxley model but with four activation steps containing forward rates 4α, 3α, 2α, α, from C_1 to O and reverse rates 4β, 3β, 2β, β from O to C_1. We show here that gating currents and ionic currents in the squid do not support such a kinetic scheme. An inability of the Hodgkin-Huxley model to fit sodium current data also has been shown with squid gating currents (Armstrong and Bezanilla, 1977), mammalian single-channel currents (Horn and Vandenberg, 1984), and the time course of development of inactivation of macroscopic ionic currents (Bezanilla and Armstrong, 1977; Oxford, 1981; Goldman and Schauf, 1972; Goldman and Kenyon, 1982).

In the extended model, the best fit was obtained when the first three transitions from closed states C_1 through C_4 had equal rates. We can then ask how these transition rates relate to the movement of the putative gating units. If we assume, for example, that the gating units are identical (i.e., they cannot be kinetically distinguished) then we can estimate the interaction between them that would give identical rates among the first four states. The derivation is presented in the appendix for the case of three identical gating units where each has two stable equilibrium states with a first order transition between them, and the derivation is similar for four identical units. The result predicts that the interaction between identical gating units is cooperative such that it becomes easier for a unit to make a transition when the other(s) have already moved. If the energy barrier for the last unit to move is ΔG, then when it is the first of three to move the energy barrier is $\Delta G + kT\ln 3$, and when one has moved already it is $\Delta G + kT\ln 2$. If four identical gating units are assumed, the first of four particles to move would have the energy barrier of $\Delta G + kT\ln 4$. This indicates that the magnitude of the interaction needed to account for identical rates is rather small. In our extended model the transitions from C_4 to C_5 to O might be accounted for by the fourth hypothetical gating unit moving in two sequential steps after the other three have reoriented, or in one step with a concerted opening transition. The parallel steps I_4, I_5, and I would correspond to the movement of the fourth unit and channel opening when the inactivation segment is in its blocking position, producing charge immobilization and inactivation of the macroscopic current.

This derivation shows that small interactions between identical gating domains could produce approximately equal rate constants for the early transitions. Alternatively, the gating particles might not be functionally identical. This suggestion is consistent with differences in the primary sequences of the four homologous domains, differences in the S4 regions, and the hypothesis that beta subunits could contribute to nonequivalence of the alpha domains. Differences in function of the domains are suggested by the experiments of Stuhmer et al. (1989) showing that mutations of the positive charges in the S4 region of domains I and II do not produce the same effects. The equal rate constants for early transition rates might then reflect a combination of parallel or sequential transition rates from the putative gating domains.

APPENDIX

Three identical particles: conversion to a sequential model

Assume that there are three identical particles (or subunits) involved in the early steps of channel opening. Each particle has two stable positions and in the diagram (Fig. A1), the left position indicates the deactivated position and the right indicates the activated position. For the channel to be primed (or ready to proceed to the open state) all three of them must be in the activated position. The particles may interact with each other, and the rate constants for transition from left to right, as indicated in the diagram, are p, q, or r, depending on the number of other particles still remaining on the left when the particle moves. Similarly, the rates from right to left are u, v, or w, depending on whether two, one, or no particles remain on the right side when the particle moves to the left.

Because the particles are identical, then states S_{2a}, S_{2b}, and S_{2c} are

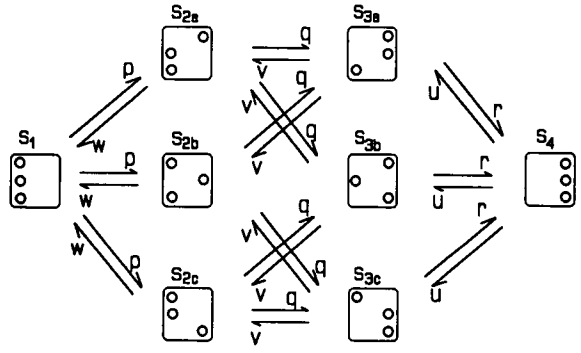

FIGURE A1 State diagram for three identical particles each having two stable positions.

indistinguishable from each other, as are states S_{3a}, S_{3b}, and S_{3c}. The model can be represented by the following:

$$S_1 \underset{w}{\overset{3p}{\rightleftharpoons}} S_2 \underset{2v}{\overset{2q}{\rightleftharpoons}} S_3 \underset{3u}{\overset{r}{\rightleftharpoons}} S_4.$$

As the particles may interact among themselves, this is not equivalent to the Hodgkin and Huxley (1952) model, but it can be reduced to it if the interaction is removed. In the absence of interaction, $p = q = r = \alpha$ and $u = v = w = \beta$ and we get

$$S_1 \underset{\beta}{\overset{3\alpha}{\rightleftharpoons}} S_2 \underset{2\beta}{\overset{2\alpha}{\rightleftharpoons}} S_3 \underset{3\beta}{\overset{\alpha}{\rightleftharpoons}} S_4,$$

which corresponds to the Hodgkin and Huxley model for Na activation if we make the primed state (S_4) the open state.

Energy barriers

We can interpret these transition rates in terms of energy barriers to assess the interaction energy. Following Eyring rate theory, the simple energy barrier diagram pictured in Fig. A2 represents the nonelectrical part of the barrier. We will assume, for simplicity that the interaction is not electrical to develop the following relations. Let us call ΔG_i the energy barrier (in absence of electric field) for the transition between states i and $i + 1$. The rate will be given by

$$a_i = A_0 \exp\left(-\frac{\Delta G_i}{kT} + \frac{z_q eV}{kT}\right).$$

For example, referring to the state scheme above, for $i = 2$ we have

$$q = a_2 = A_0 \exp\left(-\frac{\Delta G_2}{kT} + \frac{z_q eV}{kT}\right),$$

which corresponds to the forward rate of any of the particles when one has jumped and the other is still in the left position.

Then, we can ask what happens when all the rates are equal in the model. That means that $3p = 2q = r = y$. The case of $3p = y$ can be written explicitly as

$$3A_0 \exp\left(-\frac{\Delta G_1}{kT} + \frac{z_q eV}{kT}\right) = A_0 \exp\left(-\frac{\Delta G}{kT} + \frac{z_q eV}{kT}\right),$$

which implies that

$$\ln 3 - \frac{\Delta G_1}{kT} = -\frac{\Delta G}{kT},$$

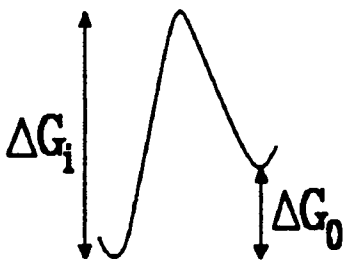

FIGURE A2 Energy barrier diagram for an isolated particle.

where ΔG is the energy barrier encountered by a particle in the absence of interaction. This means that the first transition will have a barrier $\Delta G_1 = \Delta G + kT\ln 3$. For the second transition $2q = y$:

$$\ln 2 - \frac{\Delta G_2}{kT} = -\frac{\Delta G}{kT},$$

which means that the second transition will have a barrier $\Delta G_2 = \Delta G + kT\ln 2$. For the final transition, $r = y$:

$$\frac{\Delta G_3}{kT} = \frac{\Delta G}{kT},$$

which, as expected, means that the energy barrier will be $\Delta G_3 = \Delta G$.

For the case of the return rates, they are given by:

$$b_i = B_0 \exp\left(-\frac{\Delta G_i - \Delta G_0}{kT} - \frac{z_q eV}{kT}\right).$$

Again, in the case of equal rates we have $3u = 2v = w = z$, and as derived above,

$$\Delta G_3 = \Delta G + kT\ln 3,$$

for the first transition from right to left, and the next two will be $\Delta G + kT\ln 2$ and ΔG respectively.

In general, for the sequential model with equal rates, if the barrier to jump when the particle is alone is ΔG, then when it is not alone, the barrier is increased by $kT\ln(n)$ where n is the number of particles in the same side.

We thank Drs. Richard Horn, Mailen Kootsey, and Kenneth Lange for providing computer programs that were used in the analysis, and Drs. Ana Maria Correa, Richard Horn, and Eduardo Perozo for critically reading the manuscript.

This work was supported by National Institutes of Health grants GM 30376 and HL 41656.

Received for publication 11 June 1991 and in final form 21 August 1991.

REFERENCES

Akaike, H. 1974. A new look at the statistical model identification. *IEEE (Inst. Electr. Electron. Eng.) Trans. Automatic Control.* AC-19: 716–723.

Aldrich, R. W., D. P. Corey, and C. F. Stevens. 1983. A reinterpretation of mammalian sodium channel gating based on single channel recording. *Nature (Lond.).* 306:436–441.

Aldrich, R. W., and C. F. Stevens. 1987. Voltage-dependent gating of single sodium channels from mammalian neuroblastoma cells. *J. Neurosci.* 7:418–431.

Alicata, D. A., M. D. Rayner, and J. G. Starkus. 1990. Sodium channel activation mechanisms. Insights from deuterium oxide substitution. *Biophys. J.* 57:745–758.

Armstrong, C. M. 1981. Sodium channels and gating currents. *Physiol. Rev.* 61:644–683.

Armstrong, C. M., and F. Bezanilla. 1977. Inactivation of the sodium channel. II. Gating current experiments. *J. Gen. Physiol.* 70:567–590.

Armstrong, C. M., and W. F. Gilly. 1979. Fast and slow steps in the activation of sodium channels. *J. Gen. Physiol.* 74:691–711.

Bean, B. P. 1981. Sodium channel inactivation in the crayfish giant axon. Must channels open before inactivating? *Biophys. J.* 35:595–614.

Bekkers, J. M., I. C. Forster, and N. G. Greeff. 1990. Gating current associated with inactivated states of the squid axon sodium channel. *Proc. Natl. Acad. Sci. USA.* 87:8311–8315.

Bezanilla, F. 1985. Gating of sodium and potassium channels. *J. Membr. Biol.* 88:97–111.

Bezanilla, F. 1987. Single sodium channels from the squid giant axon. *Biophys. J.* 52:1087–1090.

Bezanilla, F., and C. M. Armstrong. 1977. Inactivation of the sodium channel. I. Sodium current experiments. *J. Gen. Physiol.* 70:549–566.

Bezanilla, F., and A. M. Correa. 1991. Single sodium channels in high internal sodium in the squid giant axon. *Biophys. J.* 59:12*a*. (Abstr.)

Catterall, W. A. 1986. Molecular properties of voltage-sensitive sodium channels. *Annu. Rev. Biochem.* 55:953–985.

Chandler, W. K., and H. Meves. 1970. Evidence for two types of sodium conductances in axons perfused with sodium fluoride solution. *J. Physiol. (Lond.).* 211:653–678.

Colquhoun, D., and A. G. Hawkes. 1983. The principles of the stochastic interpretation of ion-channel mechanisms. *In* Single-Channel Recording. B. Sakmann and E. Neher, editors. Plenum Publishing Corp., New York. 135–175.

Colquhoun D., and F. Sigworth. 1983. Fitting and statistical analysis of single-channel records. *In* Single-Channel Recording. B. Sakmann and E. Neher, editors. Plenum Publishing Corp., New York. 191–264.

Correa, A. M., and F. Bezanilla. 1990. Properties of squid single Na channels in an extended voltage range. *Biophys. J.* 57:102*a* (Abstr.)

Correa, A. M., R. Latorre, and F. Bezanilla. 1991. Ion permeation in normal and batrachotoxin-modified Na^+ channels in the squid giant axon. *J. Gen. Physiol.* 97:605–625.

Gillespie, J. I., and H. Meves. 1980. The time course of sodium inactivation in squid giant axons. *J. Physiol. (Lond.).* 299:289–307.

Goldman, L., and C. L. Schauf. 1972. Inactivation of the sodium current in *Myxicola* giant axons. Evidence for coupling to the activation process. *J. Gen. Physiol.* 59:659–675.

Goldman, L., and J. L. Kenyon. 1982. Delays in inactivation development and activation kinetics in *Myxicola* giant axons. *J. Gen. Physiol.* 80:83–102.

Gonoi, T., and B. Hille. 1987. Gating of Na channels. Inactivation modifiers discriminate among models. *J. Gen. Physiol.* 89:253–274.

Guy, H., and P. Seetharamulu. 1986. Molecular model of the action potential sodium channel. *Proc. Natl. Acad. Sci. USA.* 83:508–512.

Hodgkin, A. L., and A. F. Huxley. 1952. A quantitative description of the membrane current and its application to conduction and excitation in nerve. *J. Physiol. (Lond.).* 117:500–544.

Horn, R., and K. Lange. 1983. Estimating kinetic constants from single channel data. *Biophys. J.* 43:207–223.

Horn, R., and C. A. Vandenberg. 1984. Statistical properties of single sodium channels. *J. Gen. Physiol.* 84:505–534.

Horn, R., and C. A. Vandenberg. 1986. Inactivation of single sodium channels. *In* Ion channels in Neural Membranes. J. Ritchie, R. D. Keynes, and L. Bolis, editors. Alan R. Liss, New York. 71–83.

Horn, R., C. A. Vandenberg, and K. Lange. 1984. Statistical analysis of single sodium channels. Effects of *N*-bromoacetamide. *Biophys. J.* 45:323–335.

Keynes, R. D. 1986. Modeling the sodium channel. *In* Ion channels in Neural Membranes. J. Ritchie, R. D. Keynes, and L. Bolis, editors. Alan R. Liss, New York. 86–101.

Kirsch, G. E., and A. M. Brown. 1989. Kinetic properties of single sodium channels in rat heart and rat brain. *J. Gen. Physiol.* 93:85–99.

Korn, S. J., and R. Horn. 1988. Statistical discrimination of fractal and Markov models of single-channel gating. *Biophys. J.* 54:871–877.

Kunze, D. L., A. E. Lacerda, D. L. Wilson, and A. M. Brown. 1985. Cardiac Na currents and the inactivating, reopening, and waiting properties of single cardiac Na channels. *J. Gen. Physiol.* 86:691–719.

Levis, R. A. 1988. Single Na channel currents from squid giant axon following removal of fast inactivation by pronase. *Biophys. J.* 53:226*a*. (Abstr.)

McManus, O. B., D. S. Weiss, C. E. Spivak, A. L. Blatz, and K. L. Magleby. 1988. Fractal models are inadequate for the kinetics of four different ion channels. *Biophys. J.* 54:859–870.

Nagy, K. 1987. Evidence for multiple open states of sodium channels in neuroblastoma cells. *J. Membr. Biol.* 96:251–262.

Noda, M., S. Shimizu, T. Tanabe, T. Takai, T. Kayano, T. Ikeda, H. Takahashi, H. Nakayama, Y. Kanaoka, N. Minamino, K. Kanagawa, H. Matsuo, M. A. Raftery, T. Hirose, S. Inayama, H. Hayashida, T. Miyata, and S. Numa. 1984. Primary structure of *Electrophorus electricus* sodium channel deduced from cDNA sequence. *Nature (Lond.).* 312:121–127.

Nonner, W. 1980. Relations between the inactivation of sodium channels and the immobilization of gating charge in frog myelinated nerve. *J. Physiol. (Lond.).* 299:573–603.

Oxford, G. S. 1981. Some kinetic and steady-state properties of sodium channels after removal of inactivation. *J. Gen. Physiol.* 77:1–22.

Oxford, G. S., and J. Z. Yeh. 1985. Interactions of monovalent cations with sodium channels in squid axon. I. Modification of physiological inactivation gating. *J. Gen. Physiol.* 85:583–602.

Patlak, J. B., and M. Ortiz. 1986a. Two models of late Na^+ channel currents in frog sartorius muscle. *J. Gen. Physiol.* 87:305–326.

Patlak, J. B., M. Ortiz, and R. Horn. 1986. Opentime heterogeneity during bursting of sodium channels in frog skeletal muscle. *Biophys. J.* 49:773–777.

Roux, B., and R. Sauve. 1985. A general solution to the time interval omission problem applied to single-channel analysis. *Biophys. J.* 48:149–158.

Salkoff, L., A. Butler, A. Wei, N. Scavarda, K. Baker, D. Pauron, and C. Smith. 1987. Molecular biology of the voltage-gated sodium channel. *Trends Neurosci.* 12:522–527.

Scanley, B. E., D. A. Hanck, T. Chay, and H. A. Fozzard. 1990. Kinetic analysis of single sodium channels from canine cardiac purkinje cells. *J. Gen. Physiol.* 95:411–437.

Stevens, C. F. 1978. Interactions between intrinsic membrane protein and electric field. *Biophys. J.* 22:295–306.

Stimers, J. R., F. Bezanilla, and R. E. Taylor. 1985. Sodium channel activation in the squid giant axon. Steady-state properties. *J. Gen. Physiol.* 85:65–82.

Stimers, J. R., F. Bezanilla, and R. E. Taylor. 1987. Sodium channel gating currents. Origin of the rising phase. *J. Gen. Physiol.* 89:521–540.

Stuhmer, W., F. Conti, H. Suzuki, X. Wang, M. Noda, N. Yahagi, H. Kubo, and S. Numa. 1989. Structural parts involved in activation and inactivation of the sodium channel. *Nature (Lond.).* 339:597–603.

Swenson, R. P., Jr. 1983. A slow component of gating current in crayfish giant axons resembles inactivation charge movement. *Biophys. J.* 41:245–249.

Vandenberg, C. A., and F. Bezanilla. 1988. Single-channel, macroscopic and gating currents from Na channels in squid giant axon. *Biophys. J.* 53:226*a*. (Abstr.)

Vandenberg, C. A., and F. Bezanilla. 1990. Modeling Na channels in squid giant axon from single-channel, macroscopic and gating currents. *Biophys. J.* 57:296*a*. (Abstr.)

Vandenberg, C. A., and F. Bezanilla. 1991. Single-channel, macroscopic and gating currents from sodium channels in squid giant axon. Biophys. J. 60:000–000.

Vandenberg, C. A., and R. Horn. 1984. Inactivation viewed through single sodium channels. *J. Gen. Physiol.* 84:535–564.

Woodbury, J. W. 1971. Eyring rate theory model of the current-voltage relationships of ion channels in excitable membranes. *In* Chemical Dynamics: Papers in Honor of Henry Eyring. J. O. Hirschfelder, editor. John Wiley and Sons, Inc., New York. 601–617.